

University of Alberta

DEVELOPMENT OF A MICROSENSOR TO MEASURE HUMIDITY INSIDE THE HUMAN
AIRWAYS

by

A H M Habib Ahsan



A thesis submitted to the Faculty of Graduate Studies and Research in partial fulfillment
of the requirements for the degree of **Master of Science**.

Department of Mechanical Engineering

Edmonton Alberta
Spring 2004



Library and
Archives Canada

Bibliothèque et
Archives Canada

Published Heritage
Branch

Direction du
Patrimoine de l'édition

395 Wellington Street
Ottawa ON K1A 0N4
Canada

395, rue Wellington
Ottawa ON K1A 0N4
Canada

Your file *Votre référence*
ISBN: 0-612-96440-X
Our file *Notre référence*
ISBN: 0-612-96440-X

The author has granted a non-exclusive license allowing the Library and Archives Canada to reproduce, loan, distribute or sell copies of this thesis in microform, paper or electronic formats.

L'auteur a accordé une licence non exclusive permettant à la Bibliothèque et Archives Canada de reproduire, prêter, distribuer ou vendre des copies de cette thèse sous la forme de microfiche/film, de reproduction sur papier ou sur format électronique.

The author retains ownership of the copyright in this thesis. Neither the thesis nor substantial extracts from it may be printed or otherwise reproduced without the author's permission.

L'auteur conserve la propriété du droit d'auteur qui protège cette thèse. Ni la thèse ni des extraits substantiels de celle-ci ne doivent être imprimés ou autrement reproduits sans son autorisation.

In compliance with the Canadian Privacy Act some supporting forms may have been removed from this thesis.

Conformément à la loi canadienne sur la protection de la vie privée, quelques formulaires secondaires ont été enlevés de cette thèse.

While these forms may be included in the document page count, their removal does not represent any loss of content from the thesis.

Bien que ces formulaires aient inclus dans la pagination, il n'y aura aucun contenu manquant.

Canada

Abstract

The present project is aimed at developing a capacitive humidity microsensors to measure humidity profiles inside the human respiratory tract. The ultimate goal of the project is to design the sensor with minimum size and maximum sensitivity providing minimum response time. The sensor will allow determination of humidity variation in different branches (also known as generations of airways) of the human lung during a breath. The design process involves an appropriate simulation of the sensor to investigate the influence of several parameters on its sensitivity. This sensor consists of interdigitated electrodes formed as a capacitor using gold as conductor and polyimide as dielectric built on a silicon substrate. For the thermal resetting, a polysilicon microheater is built just underneath the sensor. The system should have quick absorption of moisture and ideally have a response time of less than 1 s. In order to meet these constraints, a capacitive sensor was designed with a dielectric sensitive to humidity. All related parameters such as shapes of air contact surfaces, domain dimensions, properties of materials, etc. are analyzed and results are shown as well. Although the design and development were entirely numerical, preliminary manufacturing work was performed and recommendations for complete manufacturing protocols are included.

To my dearest God.
To my loving parents.

Acknowledgements

I would firstly like to extend my sincerest thanks to my supervisor Dr. Carlos F. Lange for his direction and patience during the completion of this manuscript. I acknowledge him for the research experience I have acquired by his extraordinary guidance associated with his vast knowledge of research work and numerical simulations.

Secondly, I would like to acknowledge Dr. Walied Moussa for his support and guidance, Prof. Volker Saile (Institute of Microstructure Technology, Germany) who was generous enough to provide me with relevant literature from his students, Dr. Chris Backhouse for his valuable suggestions, Dr. Edgar Matida and Dr. Ken Westra for the valuable discussions.

I would like to thank my lab mates, colleagues and friends for my many questions and interruptions of their work. My thanks specially go out to Andrew Martin, Biljana Grgic, Dr. Edgar Matida, Yu Zhang and Dr. Zhaolin Wang. I would like to thank Helena Orszanska and all of my lab mates for creating a rich and delightful research environment in our lab – the Aerosol Research Laboratory of Alberta (ARLA).

I would also like to say that I owe my parents an enormous debt of gratitude. They taught me the value of hardwork, honesty and loyalty. Their love and support has always given me the drive to excel.

Finally, I would like to thank the Department of Mechanical Engineering and the Natural Sciences and Engineering Research Council of Canada for financially supporting this work.

Contents

1	Introduction	1
1.1	Objective	2
1.2	Microsensors	2
1.3	Advantages	2
1.4	Capacitive Microsensors	3
1.4.1	Dielectric Constant, ϵ_r	5
1.5	Humidity Sensors	5
1.6	Correlation between ϵ_r and %RH	7
1.7	Capacitive Humidity Microsensors	8
1.7.1	Polymer Sensors and Polyimide	8
1.7.2	Polyimide	10
1.7.3	Importance of the Humidity Microsensor	10
2	Governing Physics	12
2.1	How Capacitive Microsensors Work	12
2.2	Diffusion Process	13
2.2.1	Relative Permittivity	14
2.3	Electroquasistatic	15
2.4	Calculating Capacitance	16
2.5	Multiphysics	17
2.6	Microheater for Thermal Reset	18
3	Simulation/Modeling	20
3.0.1	Response Time	20
3.0.2	Integrated Water Vapor Mass	20
3.1	Description of the Sensor	20
3.1.1	Thin layers and dimensions	21
3.1.2	Materials and properties	21
3.2	FEMLAB and MATLAB: simulation software	22
3.3	Simulation Domain	23
3.4	Assumptions	23
3.5	Simulation Model	24
3.6	Boundary Conditions and Multiphysics	25
3.6.1	Dirichlet and Neumann	25

3.6.2	Multiphysics	27
4	Parameter Study	28
4.1	Diffusion	28
4.1.1	Diffusion Coefficient, D	29
4.1.2	Height of the Subdomains	29
4.1.3	Width of the Effective Subdomain	30
4.1.4	Air Contact Surface of the Polyimide	30
4.2	Electrostatics	30
4.3	Diffusion: Parameter Study	30
4.3.1	Surface Geometry	30
4.3.2	Domain Geometry	34
4.4	Electrostatic: Parameter Study	35
4.4.1	Air Subdomain	35
4.4.2	Domain Geometry	36
4.4.3	Varying Dielectric Width (W_p)	38
4.4.4	Varying Electrode Height (t_e)	41
4.4.5	Varying Electrode Width (W_e)	43
4.5	Grid Resolution and Time Step Resolution	44
4.6	Analytical Verification	44
4.6.1	Diffusion	45
4.6.2	Electrostatic	47
4.6.3	Thermal	47
4.7	Summary of Results	48
5	Microfabrication	50
5.1	Selection of Specimens	50
5.2	Selection of models to be micromachined	50
5.3	Micromachining in MicroFab Lab	52
5.3.1	Ledit	53
5.3.2	Mask making	53
5.3.3	Pattern transfer: microheater and microsensor structures	56
5.3.4	Dispensing polyimide and curing	57
5.3.5	Providing a desired shape to the polyimide flat surface	58
6	Conclusion	60
A	Tables	62
B	Figures	64
C	Matlab Codes	65

List of Figures

1.1	Polymer sensors with narrow [left] and wide [right] electrode gaps.	9
2.1	Electric fields or flux lines for parallel plates [3].	13
3.1	A 2D symmetric view of the system.	21
3.2	Approach on 2D domain.	23
3.3	Total and Effective Subdomains.	25
3.4	Boundary conditions applied in Diffusion mode.	26
3.5	Boundary conditions applied in Electrostatic mode.	27
4.1	Dimensions of the subdomains.	29
4.2	Different shapes and dimensions used in the parameter study.	31
4.3	Water vapor accumulation in effective subdomain over time.	32
4.4	2D view of diffusion solution and electric field in Dim4 at steady state.	33
4.5	System with air subdomain. Arrows indicate the electric field.	36
4.6	Surface diagram of Electric Potential in the system of Dim4.	37
4.7	Total electric field as a function of thickness of the air subdomain.	38
4.8	Capacitance against dielectric width.	39
4.9	Electrical energy variation for different dielectric width.	40
4.10	Capacitance against electrode height.	41
4.11	Total sensor capacitance against electrode width.	44
4.12	Model1 for analytical calculations.	45
4.13	Simulation results in a cross section line plot along the vertical line at the middle of the model.	46
4.14	Time dependent analytical and simulation diffusion solution for the point on y at the top of the effective domain in Model1.	47
4.15	Thermal domain in the sensor system.	48
5.1	A full MEMS structure.	51
5.2	Three sensors in a full MEMS structure.	52
5.3	Four sensors in a full MEMS structure.	52
5.4	One cell composed of 6 sensors structure. Electrical connection points are seen on the right half of the cell.	53
5.5	8-cells layout of the combined structure on a wafer.	54

B.1	Air contact surface temperature with time for different heat fluxes generated by the microheater.	64
-----	---	----

List of Tables

4.1	Results: Dim4 to Dim8 at steady state.	34
4.2	Results: Domain geometry study on Dim4 for diffusion.	35
4.3	Results: Domain geometry study on Dim1 for diffusion.	35
4.4	Air properties used.	36
4.5	Results: Domain geometry study on Dim4 for electrostatics.	37
4.6	Results: Varying W_p on Dim1.	39
4.7	Results: Varying t_e on Dim1 with $W_p = 10 \mu\text{m}$	42
4.8	Results: Varying t_e on Dim1 with $W_p = 5 \mu\text{m}$	42
4.9	Results: Varying W_e on Modell with W_p at a minimum.	43
5.1	Specimens for micromachining.	51
A.1	Additional methods of micromachining surface of polyimide film.	62
A.2	Material properties [24, 5] used in the simulation.	63
A.3	List of polyimides with specifications.	63

Chapter 1

Introduction

For long time aerosol technology has been serving an important, albeit inefficient contribution to the medical sciences for treatment of pulmonary diseases such as asthma. Recent research aimed at providing a better scientific foundation to aerosol delivery is highly dependent on the transport phenomena inside the lungs - how air or aerosol particles are distributed along the air passages inside the lungs.

For inhaled pharmaceutical aerosols, particle size affects their own deposition in the respiratory tract. In fact inside the human airways these particles absorb or lose mass from their surface due to evaporation or condensation. These hygroscopic¹ size changes are caused by the interaction of water molecules at the air-water interface. They occur due to the existence of significant amount of gradients in water vapor concentration in the air next to a droplet surface. The physical problem becomes interesting and rather challenging when these effects are actually seen in many droplets in a volume of air rather than in a single droplet only. Finlay in his book [11] shows that when many droplets are present in a given volume, the droplets are affected by the ambient air. This ambient air is then in turn affected by the evaporation or condensation of these droplets. Hygroscopic size changes occurring under such conditions are referred to as 'two-way coupled' hygroscopic effects [11] in the distribution of polydisperse inhaled pharmaceutical aerosols. For an accurate simulation of the coupled heat and mass transfer problem between the air and hygroscopic aerosols in the lung, the temperature and humidity as well as the heat and mass transfer coefficients at the airway walls have to be known. Some studies have tried to measure conditions in the airways for various breathing patterns and inhaled air conditions, and infer wall temperatures and transfer coefficients through mathematical models [10]. McFadden et al. [25] were the first to obtain a thermal map of the airways in the human respiratory system using a series of thermistors. Their results were then used by Daviskas et al. [7] to estimate (using energy balance equations) the airway wall temperature and the heat transfer coefficient at each lung generation.

¹Due to water being the substance that is transferred at the surface of the particle, the size changes in particles can be termed hygroscopic size changes.

In a similar fashion a humidity sensor is being developed in this project, which will serve to construct a humidity map of the human airways, and to obtain the corresponding mass transfer coefficients.

1.1 Objective

The objective of this work is to develop a humidity microsensor and optimize the design to ensure a short response time to serve the purpose of using it in human airways. The development and optimization are entirely based on numerical simulation of the sensor. The response time is aimed to be as short as it is viable to measure the humidity profile in the different generations (also known as branches in human the airways) in a single breath. Since a single inhalation can take up to 4 s, a response time of less than 1 s is targeted in this project. Response time of a capacitive humidity microsensor can be shortened either by choosing a dielectric substance with higher diffusion coefficient or by changing the shape and dimensions of all the sensor parts. Hence, in this project a comprehensive numerical parametric analysis is performed on the polyimide layer and electrodes to identify a sensor design that minimizes response time and maximizes sensitivity.

1.2 Microsensors

The microelectronics revolution with regard to measurement systems is characterized by increasingly complex signal-data processing chips associated with falling costs. Various microsensors being developed are examples of this revolution. A microsensor is a sensor that has at least one physical dimension at the submillimeter level.

1.3 Advantages

There is a two-pronged benefit in any microsensor development:

- it reduces the size of the device
- decreases cost of production

As a result the marketability of sensors has become wider leading to an increase in its applicability through lower weight, lower manufacturing cost and wider range of applications. This applicability inspired the industries to manufacture microsensors in volumes, if necessary, with integrated microelectronic circuitry. Now it is all about fabricating monolithic or integrated chips that can not only sense but also actuate to create a microsystem that encompasses the information-processing triptych² [12]. This technology

²information-processing triptych – a combination of sensor, processor and actuator working together in a microsystem

is called microsystems technology (MST) which is being added with microelectromechanical systems in microfabrication. In fact an advanced and attractive solution to the development of microelectromechanical systems (MEMS) is to make all its techniques compatible with silicon processing. Therefore, combining CMOS³ processing with microsystems technology has become a significant approach. Dramatic advances in MEMS, being the next logical step in the silicon revolution, over the last few years began to show a glimpse of the new silicon revolution. The microsensors research covers diverse disciplines such as materials, microfabrication, electronics, and mechanics. Among different types of sensor technologies, the capacitive type is found to be predominant in measurement systems in the microlevel. A brief understanding about capacitive humidity microsensors can be obtained in following sections.

1.4 Capacitive Microsensors

For a given application a capacitive sensor can be made unaffected by temperature, humidity, or mechanical alignment, and shielding against stray electric fields is simple compared to shielding an inductive sensor against magnetic disturbance [3]. In case of sensitivity and stability, a capacitive sensor is ten times better [3] than traditional silicon-based sensor technologies.

Baxter's 'Capacitive Microsensors, Design and Applications' [3] and Gardner's 'Microsensors: Principles and Applications' [12] offer invaluable information and advice regarding efficient capacitive microsensor structure and electrode arrangements, among others. In addition, several recent research works in this field were relevant in the process of reaching a decision of selections and design.

In the work of Domansky et al. [8] the dielectric response in chemical sensors based on mesoporous silica films was monitored. As a part of this work they experimentally showed upon presence of water vapor both dielectric constant and dissipation factor increase. They found the dielectric constant varies with relative humidity approximately linearly but the dependence of dissipation factor on relative humidity (RH) is not linear.

In 2000, Matsuguchi et al. in their work [22] gave importance to the drift phenomenon of the humidity sensors by aging in hot and humid atmosphere. A method was developed to ensure a stable and reliable capacitive-type humidity sensor. In terms of sensing mechanism, changes in sensing polymer's water sorption characteristics over time can lead to changes in the sensor's dielectric properties. Long time hydrolysis of a polyimide film in presence of moisture and heat changes the polarizability and water-sorption properties of the film. This drift phenomenon is seen to happen in some linear polyimides. But some hydrophobic polymers, which absorb water vapor and in which the sorbed water stays in a vapor like state are suitable as stable capacitive-type sensors in a hot and humid atmo-

³Complementary Metal Oxide Semiconductor

sphere. According to the authors PMMA⁴ and PI⁵ meet this requirement and are suitable for practical and reliable sensors. In 2002 Matsuguchi with other coworkers published a study [23] on sorption of water vapor and CO₂ in a capacitive-type humidity sensor. In this work they used a highly crosslinked⁶ polymer named PVCA⁷ as dielectric material. They also examined the influence of coexisting CO₂ gas in air on the humidity sensor output.

In a paper [31], authored by Qu et al., a semiconductor metal oxide MnWO₄ was used as a dielectric to develop a thick-film humidity sensor. Porous MnWO₄ ceramic layer doped with LiCl was sandwiched by two interdigitated metal films forming a parallel plate capacitor arrangement. They proposed a novel electrode arrangement and could obtain high sensitivity and a short response time. According to their conclusion, the sensor characteristics were affected greatly by conditions in micromachining. However MnWO₄ ceramic layers show high porosity but do not compromise mechanical stability. In another paper [30] the same authors mentioned that ceramic humidity sensors using thick-film technology were not yet successful due to the difficulties in fabricating a suitable pore structure for the dielectric.

Rittersma et al. [32] developed a capacitive humidity sensor using a porous silicon dielectric film. The device consisted of a parallel plate capacitor combined with two integrated resistors. There were two metal resistors for measuring the temperature of the sensor, and a metal refresh resistor for controlling the amount of vapor absorbed.

In 1999 and 2001 two important papers [41, 40], relating development of a humidity microsensor, were authored by Wu et al. By a deposition technique called GLAD (Glancing Angle Deposition) they developed a humidity sensor with SiO being the dielectric film. This sensor could exhibit a response time of less than 3 s for a stepwise change in *RH* from 15% to 80%.

A capacitive sensor consumes very little power showing a lifetime of several years. Capacitive sensors in microlevel are being developed these days for their easy integration, linear characteristics and wide application ranges for different critical geometries besides all other advantages they present. For proximity detection and measurement systems capacitive microsensors are overcoming all other types of technologies day by day. Development of switches, communications, computer graphic input, for instance, are also other applications where a capacitive microsensor is playing an efficient vital role. The working principle of a capacitive microsensor is described in section 2.1.

If the dielectric material is a conductor it is easy to measure the conductivity by some

⁴PMMA – polymethyl methacrylate

⁵PI – cross-linked polyimide

⁶polymers, which have a carbonyl group as a weak hydrophilic site

⁷Poly-vinyl Cinnamate

circuit arrangement. Usually dielectric materials are nonconductive but in reality most materials are neither the one nor the other. They possess both conductance and capacitance. When an attempt is made to measure these quantities using alternating current of various frequencies, the values of conductivity vary so much with the frequency that they become insignificant as output signals. So, capacitance would be the main output parameter of interest.

1.4.1 Dielectric Constant, ϵ_r

Dielectric Constant (ϵ_r , also known as permittivity, DK, Er, etc.) is the property of a material that determines the relative speed that an electrical signal will travel in that material. Signal speed is roughly inversely proportional to the square root of the dielectric constant. A low dielectric constant will result in a high signal propagation speed and a high dielectric constant will result in a much slower signal propagation speed.

Dielectric constant is not an easy property to measure or to specify, because it depends not only on the intrinsic properties of the material itself, but also on the test method, the test frequency and the conditioning of samples before and during the test. Dielectric constant tends to shift with temperature [36, 8].

In IC (integrated circuit) technologies the characteristic impedance of a PWB⁸ is determined by the thickness of the laminate (spacing between copper layers) and its dielectric constant. Impedance control, and impedance matching of critical linked functional modules are especially important in very high speed devices and designs.

Dielectric constant is a major parameter in a capacitive device. Different types of materials are being used in the market as dielectrics in capacitive devices. Several types of polymers are available in the market for these purposes, specially for sensor technologies. A capacitive sensor made up of polymer dielectric is called a polymer sensor. Some features about polymer sensors are focused in section 1.7.1.

All the fundamental knowledge presented above is taken into account in order to maximize the output of a capacitive microsensor. In particular, the fact that a change in geometry or in the dielectric constant can change the value of capacitance allows a microsensor to become a transducer.

1.5 Humidity Sensors

Humidity sensors determine the density or pressure of water in vapor form. It can be done either by measuring relative humidity or dewpoint temperature. The common methods for measuring vapor density in the atmosphere are [38]:

⁸Printed Wiring Board, also called PCB

1. Chilled mirror method
2. Film polymer capacitance method
3. Psychrometric method

The chilled mirror method uses a metallic mirror with good thermal conductivity. The mirror is chilled using a thermoelectric cooler until dew just begins to form. A beam of light (from a solid-state LED) is aimed at the mirror surface. By monitoring the reflected light with a photodetector, water vapor content in surrounding gas can be measured.

The film polymer capacitive method uses a capacitive sensor to measure the relative humidity of the surrounding gas. In this capacitive sensor a special type of polymer is used for a specific application. As polymers absorb gas or fluid from the surroundings the type of polymer to be used is based on the type of fluid or gas to be measured.

The psychrometric method uses an instrument used for measuring the water vapor content of the atmosphere. It consists of two thermometers (the dry bulb and the wet bulb). When the bulbs are suitably ventilated, they indicate the thermodynamic wet- and dry-bulb temperatures of the atmosphere. A psychrometric chart is consulted to calculate the relative humidity of the atmosphere corresponding to these two temperatures.

Though chilled mirror method is considered the golden standard as it provides maximum precision, it is comparatively costly. The psychrometric method is seen to be very inefficient nowadays. Of these three, the film polymer capacitive method is often preferred for its linear characteristics along with very low cost. This method allows a sensor to have electrical signal or voltage outputs, which lends itself to remote monitoring of the relative humidity.

The disadvantages of the psychrometric type of sensor in microscale are that a) errors would be introduced if the water is contaminated, if the water supply to the wick becomes low or the reservoir runs dry, b) in extremely dry environment it is difficult to keep the wick wet, while wet bulb reading can be altered due to salty environments, c) accuracy is highly affected by air speed past the wet bulb. But once psychrometric methods were commonly used for the purpose of humidity measurement. An attempt to miniaturize a psychrometric sensor is seen in Eisner and Martonen's paper [9], where they gave particular attention to future applications in the human respiratory system. In their research work a microsensor was developed to determine temperature and humidity patterns within an airstream by using the psychrometric method. An algorithm was used to determine the water vapor pressure and subsequently, the *RH* (Relative Humidity) in the medium. Nevertheless, the authors tried to consider it for physiologically realistic simulation of the transient temperature variation within the human respiratory system. Because of all the disadvantages cited psychrometers for humidity measurement are currently being replaced by more convenient methods such as those stated above.

A remarkable attempt to develop a humidity microsensor is described by Laville et al. [20], where the sensor consists of interdigitated electrodes to have quick absorption with an ideally short response time of less than 1 s. Laville et al. in this research work used silicon as substrate, aluminum as conductor and polyimide Ultradel as dielectric. Here a sensor was manufactured according to standard CMOS processes with three different values for electrode width. They could reach their goal with a very thin height of an electrode structure and comparatively thicker layer of polyimide over it. To measure the capacitance a built-in oscillator was added to their sensor system.

A high speed capacitive humidity sensor was recently developed by Kang and Wise [18], with which they achieved a response time of 1 s. Several polyimide columns of few micron diameter were arranged in between two electrode plates so that the diffusion of moisture could occur circumferentially obeying Fick's law. A polysilicon heater was included for purposes of preventing condensation when the sensor remains inoperative, also for self-test in the field to reduce the recovery time after wetting. This process will be referred to as thermal reset later in section 2.6. Recovery of the sensing film from contamination, aging and hysteresis was also done with the help of this microheater.

Hence, a capacitive sensor can be selected and declared as the preferred type of humidity sensor satisfying the requirements of high sensitivity, short response time, small hysteresis, low cost, and low power consumption [33].

1.6 Correlation between ϵ_r and $\%RH$

An extensive search for a relationship between dielectric constant, ϵ_r , and the moisture content in dielectric materials was performed. This relationship is necessary to simulate the whole system where both electrostatic and diffusion process are coupled within the simulation. A thorough literature review revealed that it is difficult to define the proper relationship between ϵ_r and $\%RH$ [29, 4, 15].

Papazyan et al. [29] from Royal Institute of Technology, Sweden, used a formula in their research work that concerned water ingress in a mass impregnated cable. This formula was referred to by Landau [19] in 1960 in his book on electrodynamics of continuous media. A detailed view of this formula and its ineligibility to our work is explained in section 2.5 (see page 17). However, in 2001, Castela and Simoes [4] assessed water uptake in polymeric coatings by capacitance measurements. For their work they had to use an expression for the mixed dielectric constant referred to by an important paper that came at last to light. In this work authors Hartshorn et al. [15] demonstrated details of basics of diffusion processes along with concerned correlations. They experimentally proved changes in electrical properties in protective films during different diffusion processes. Three types of expressions for the mixed dielectric constant of absorbent were found for three different diffusion strategies. These expressions (see section 2.5) would be sufficient to realize an accurate relationship required for the simulation of the coupled

multiphysics system in our project. These correlations, however, came too late to make them useful in the present development.

1.7 Capacitive Humidity Microsensors

A capacitive humidity device is developed on basis of the permittivity change (change of the dielectric constant) of the material in between two electrodes. A relatively small change in humidity results in a capacitance change large enough for a sensitive detection. But there are many additional advantages when compared to others [3]:

- It enjoys wide dynamic ranges, from 0.1 ppm to saturation point.
- Ability to function accurately and reliably extends over a wide range of temperatures and pressures.
- Exhibits low hysteresis and high stability.
- Minimal maintenance required.

These features make capacitive humidity sensors viable for many specific operating conditions and ideally suited for a system where uncertainty and unaccounted conditions exist during operations.

As the dielectric constant may be highly dependent on the temperature, accurate temperature measurement is required. Usually these devices can work in the temperature range of 0 – 50°C and provided with tight temperature compensation circuit. Such a circuit is not included in the present development, because it is expected to form a separated part of a multisensor probe (see section 1.7.3).

In polymer type capacitive humidity sensors, by careful design the capacitance can be made directly proportional to percentage relative humidity of the surrounding atmosphere. Above all, a polymer type capacitive sensor is preferred by researchers due to its chemical stability. This means that contamination with air or surroundings can hardly affect the sensor element. A discussion on polymer sensors is needed at this point.

1.7.1 Polymer Sensors and Polyimide

The dielectric constant of some materials varies with temperature or the content of absorbed gas or fluid and can be used to form the basis of a sensor. If it is water vapor that diffuses into the dielectric, the value of ϵ_r can rise near to the dielectric constant of water which is relatively high (ϵ_r for water is around 80). Some polymer substances are porous enough to absorb moisture satisfactorily. When this moisture absorbs into the nonconducting polymer, it changes the dielectric constant of the material and, hence, the capacitance changes. There are two mechanisms by which a polymer sensor can work [13] regarding the swelling of its material.

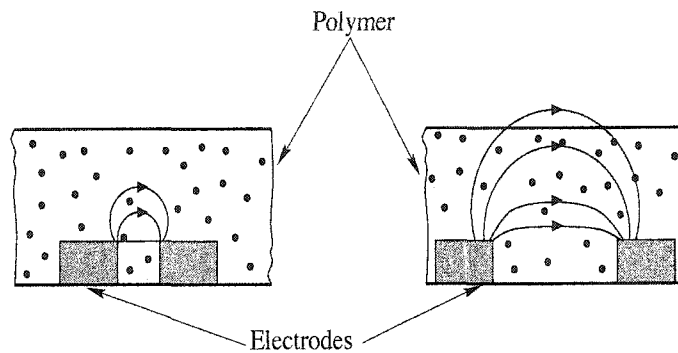


Figure 1.1: Polymer sensors with narrow [left] and wide [right] electrode gaps.

1. No effect of swelling
2. With swelling effect

No effect of swelling

When the active material (such as dielectric) is a polymer, dissolving of a foreign fluid or gas changes ϵ_r of this material. This dissolution can cause swelling of the polymer layer. In the case of a narrow electrode gap (Figure 1.1, left), if the polymer swells, the electric field is still confined in its own region in between two electrodes. As a result, whenever the polymer swells, the swelling does not change the output signal, making the design easier. Usually for the electrodes separated from each other by a very short distance, the electric field remains confined despite swelling of the dielectric.

With swelling effect

In the case of widely separated electrodes (Figure 1.1, right) the output signal will measure the entire swelling that is taking place. For wide gapped electrodes the electric field is not confined within the film. In this case as the polymer swells, the amounts of electric field confined inside and outside the dielectric are changing. Moreover, swelling in water sometimes changes the dimensions resulting in anisotropy in the material. Therefore, the output signal starts showing changeable characteristics due to swelling in addition to other effects. Solution of a design where swelling effect exists becomes difficult to predict.

A thorough review of the literature revealed that a special type of polymer named polyimide can work efficiently in a capacitive humidity sensor as the dielectric. A complete view of characteristics are explained in section 1.7.2.

1.7.2 Polyimide

When polymers are based on organic residues linked in a linear fashion via cyclic imide functionalities they are called polyimides. These cyclic imide functionalities are based exclusively on tetracarboxylic acids⁹ or their derivatives and diamine¹⁰ monomers¹¹. The high performance polyimides being used in semiconductor industries are those composed of aromatic structures [37]. Here these polymers are provided with high thermal stability, good mechanical and electrical properties. Some important properties of polyimides can easily be controlled to make it attractive as a dielectric substance for a capacitive humidity microsensor.

The reasons behind choosing polyimide for a capacitive humidity microsensor are [12]:

- Its dielectric constant is highly sensitive to humidity and the variation of its dielectric constant against relative humidity is almost linear [18, 20]. This is an important behavior of polyimide with regard to moisture. A non-linear %RH and ϵ_r relationship would be an unpredictable trouble in an efficient sensor development.
- It has high thermal stability (> 400°C). Higher thermal stability can easily confirm wider application range of the sensor. This can be an important criterion during microfabrication processes, which may involve elevated temperatures that can damage thermal and electrical properties of a material with low thermal endurance.
- Its high resistance to most chemicals ensures that the sensor can work either in toxic settings or even in very sensitive environments.
- Being a coating material developed for the semiconductor industry, polyimides are fully compatible with silicon processing technology.

The following sections describing humidity microsensors will explore the importance of developing the polymer sensor for humidity measurement by capacitive methods.

1.7.3 Importance of the Humidity Microsensor

The motivation to develop the humidity microsensors with very short response time came from the demand of present cutting-edge research concerning atmospheric determinations in the lungs during a breath. This project is part of the development of a novel multisensor microprobe [1] to measure simultaneously temperature, humidity and velocity profiles inside a human respiratory tract. Here firstly humidity, temperature and velocity microsensors are being developed separately to ultimately combine them into a single integrated chip. Since the microprobe will involve a separate development of a temperature microsensors, which can also be used for temperature compensation, there is no need to include a temperature compensation circuit in the present humidity microsensors design.

⁹Organic acids containing the carboxy (-COOH) group, including amino acids and fatty acids.

¹⁰A compound containing two amido groups united with one or more positive radicals.

¹¹A single molecule that is the subunit of a polymer.

Lung diseases, aerosols and microprobe

Lung diseases are the most common causes of death in North America and represent a growing public health issue in countries around the world. Nowadays many aerosols are commonly used as a means of delivering therapeutic drugs to the lung for the treatment of lung diseases. Prediction of deposited dosages of these inhaled pharmaceutical aerosols is an important component of the development of new inhaled drugs and new drug inhalation devices. In aerosol therapy, for an accurate simulation of the deposition of hygroscopic aerosols in lung, humidity, temperature and velocity profiles in the airways have to be known [11]. This will require a microprobe [1] with several microsensors that is not currently available in the market. The measured parameters (RH, T, V) will be used to accomplish a systematic mapping of the conditions within the respiratory tract of human test subjects, including healthy volunteers as well as patients with lung diseases.

Aerial Marker

The microprobe being developed will be unique and will also be used in the future to study the correlation between healthy and diseased profiles in human lung to try to diagnose phase and progress of a disease. In this way an '*Aerial Marker*' [1] can be invoked to predict details of the disease. There are many significant physical alterations caused by lung diseases that can affect atmospheric condition in the respiratory airways at every instant and tend to grow rapidly with time. So, early diagnosis would be possible with this new technology and it is a very important issue in every lung disease.

Microprobe and bronchoscope

As airways branch inside the lung they quickly become smaller. At the sixth branch, also called lung generation, the approximate airway diameter is only 5 mm [11]. In order not to block the air flow in the airway that is being measured the microprobe size will be limited to a square of 1 mm side. The humidity sensor is expected to occupy most of the area of this microprobe [1].

In addition to the airway side constraint, there is a vacated channel of 2.8 mm diameter in a fiber optic lung bronchoscope. This 1 mm² size of the probe will allow it to routinely be used in clinical application by inserting it through this vacated channel.

To meet the necessity of having a very short response time the sensor should perform a very swift absorption of moisture by an efficient diffusion process. In the following chapter a comprehensive discussion on diffusion is made in order to determine how the diffusion process can be expedited.

Chapter 2

Governing Physics

This chapter describes the physics involved in the present development, in particular, the principles of capacitive microsensors, diffusion process, electroquasistatic, calculation of capacitance, multiphysics and microheating.

2.1 How Capacitive Microsensors Work

For the simplest case of a parallel plate geometry where a dielectric separates the electrodes, a voltage V can be applied to the plates to produce a total flux Ψ (displacement charge) which is expressed as

$$\Psi = Q = CV \quad (2.1)$$

Here Ψ is the amount of flux in coulombs produced by V volts and C is the capacitance of the plates in coulombs/volt.

Therefore with dl , an elementary length along a flux line of displacement current, capacitance C can be calculated by evaluating [14, 3]

$$C = \frac{\epsilon_0 \epsilon_r \Psi}{\int \mathbf{D} dl} = \frac{\Psi}{\int \mathbf{E} dl} \quad (2.2)$$

Where ϵ_0 = electric permittivity of vacuum and ϵ_r = relative dielectric constant or electric permittivity of dielectric material, \mathbf{D} = current displacement, and \mathbf{E} = electric field. This integral gives the capacitance of an elementary volume surrounding the flux line, and must be repeated for all flux lines emanating from one of the plates and terminating in the other plate.

Therefore \mathbf{E} is proportional to Q , so also is V and the constant of proportionality can be called the capacitance of the arrangement [3]

$$C \equiv \frac{Q}{V} \quad (2.3)$$

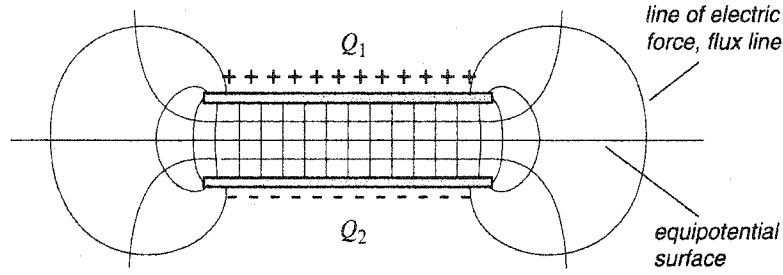


Figure 2.1: Electric fields or flux lines for parallel plates [3].

Capacitance is a geometrical quantity, determined by the sizes, shapes, and separation of the two conductors. Capacitance (C) also depends on the dielectric material. C is measured in farads (F) and more practical units are the microfarad, μF (10^{-6}F) and the picofarad, pF (10^{-12}F). If Gauss' law can be applied to a surface surrounding one of the parallel plates neglecting the fringing flux lines at the edge of the plates the capacitance results in [14, 3]

$$C = \frac{\epsilon_0 \epsilon_r A}{d} \quad (2.4)$$

Where A is the area in m^2 and d is the distance in between the plates in m.

If all the geometries are kept constant capacitance will come up as a function of electric permittivity of the dielectric, ϵ_r . Consequently, any phenomenon that changes the dielectric constant, ϵ_r will cause a change in the capacitance δC . This variation can be defined by the total differential formula [12],

$$\delta C = \left. \frac{dC}{d\epsilon} \right|_{A,d} \delta\epsilon \quad (2.5)$$

If dielectric media in a capacitor absorbs fluid, the value of ϵ_r starts changing. Several factors may be responsible for this. A detailed view of these factors and their effects are described in the following section exploring the physics of diffusion processes.

2.2 Diffusion Process

Diffusion can be defined as the random distribution of an ensemble of particles from a highly concentrated region to another with lower concentration. Fick's first law follows the equation (in x -direction) [34, 6]

$$J_x = -D_x \frac{\partial \Phi(x, t)}{\partial x} \quad (2.6)$$

Where J is the flux of mass, D is the diffusion coefficient, Φ is the concentration of the solute, x is the distance into a solid layer and t is the diffusion time. The physical

meaning of this equation is that the diffusing mass flows in the direction of decreasing concentration with time. Conservation of mass is expressed as follows

$$\frac{\partial \Phi}{\partial t} = -\nabla \cdot \mathbf{J} \quad (2.7)$$

The expression shows the rate of change in concentration in time corresponds to diffusion over a distance with the mass flux going in the direction of low concentration. And the above equations become the expression of Fick's second law of Diffusion [6]

$$\frac{\partial \Phi}{\partial t} = \frac{\partial}{\partial x} \left(D_x \frac{\partial \Phi}{\partial x} \right) + \frac{\partial}{\partial y} \left(D_y \frac{\partial \Phi}{\partial y} \right) \quad (2.8)$$

One initial condition and two boundary conditions will be required to solve Fick's Law in the simulation.

2.2.1 Relative Permittivity

Diffusing of fluid in a polymer depends on homogeneity, permittivity, dimension and swelling of polymer material at the time of diffusion. Permittivity of a given type of polymer film is inversely proportional to its thickness while considering the films being homogeneous. Because of this several studies on diffusion of water in polymers revealed features not noticed in sorption of gases or organic vapors. Diffusion related properties of a polymer are found to be greatly dependent on the details of its preparation as well. The effect of swelling of absorbent was already discussed in section 1.7.1. Hence, diffusion process involves not only simple diffusion, but also some of the above mentioned physical properties of the absorbent. If the dielectric is the absorbent in a capacitive device, its electrical property ϵ_r (relative permittivity), will be another concern. Two types of environmental factors are necessary to be focused here – Relative Humidity (%RH) and Temperature (T), which influence electrical output signals of a capacitive humidity sensor. The basic effects of %RH and T on relative permittivity (ϵ_r) of a dielectric can be described as follows:

ϵ_r Changes with Relative Humidity

For a more relevant discussion the term Electrical Displacement in a material should be introduced at first. When a nonconducting material acts as a dielectric in between two electrodes and a voltage is applied, the material will experience an electrical field. Every charged particle in this material experiences a force that is proportional to the electric intensity or voltage gradient. The charges are bound to definite positions and are capable of displacement by an electric force. The displacement of the charges determines the amount of charge and therefore the dielectric constant of the material [15].

Water, being a material with polar molecules, faces outstanding electrical displacement, which is obtained through the rotation of molecules as a whole. It may happen

even for the distortion of its internal structure. Water has a very high dielectric constant at ordinary temperatures and its molecules start rotating under the action of an electric field [15]. If the dielectric constant of a material such as polyimide, which absorbs considerable amount of water, is measured as it takes up successive measured quantities of water, the value of dielectric constant will be somewhere between the two dielectric values of pure polyimide and of water. This resultant dielectric constant can be called 'mixed dielectric constant' ($\epsilon_{r\text{mix}}$) (see section 2.5 for the expressions). Experiments show [15] that the dielectric constant of the water first absorbed is comparatively low but as more water is taken up the value gradually approaches that for ordinary water. It is evident that the water molecules first absorbed are capable of rotation to a very limited extent only. And the dielectric constant of successive layers increases until a certain thickness is reached, at which point the molecules will have the same freedom of rotation as ordinary water and, therefore, the same dielectric constant. This is why it would be best to let the diffusion reach a steady state in order to make the system more reliable. At this steady state the dielectric constant of absorbed water can be considered as that of ordinary water.

ϵ_r Changes with Temperature

Under the action of an electric field the dielectric constant of a material such as water, which is composed of polar molecules, is eagerly due to rotation of its molecules. A rise in temperature increases the forces of thermal agitation, which tend to give the molecules a random distribution of orientation and, therefore, reduces the resultant electrical displacement in the direction of an applied field [15]. Thus, the dielectric constant diminishes rapidly with rise of temperature. On the other hand, dielectric constant of pure nonconducting polymers, such as polyimide, plastics, etc. is proved to increase with a rise in temperature [15].

In other words, the change of dielectric constant with temperature observed in polar liquids is opposite to that observed in polymers. These effects could potentially compensate each other in a capacitive humidity sensor. The effect of temperature in the present development is not studied because the working temperature throughout the whole system is kept constant at a nominal value.

2.3 Electroquasistatic

Though electrostatics deals with nonmoving electrical charges, electric conductors and dielectrics, and DC potential sources, practical capacitive sensor design involves moving charges, partially conducting surfaces and AC potential sources. Hence, for an accurate analysis of the fields and currents that make up a capacitive sensor, Maxwell's equations relating electric and magnetic fields, charge density, and current density should be used.

Fortunately, a simplifying approximation, which ignores magnetic fields is almost always possible with insignificant loss of accuracy. Maxwell's equations describe the

most intricate electromagnetic wave phenomena. Analysis of such fields is difficult. In order to avoid this difficulty, a simplification is needed. Systems in which the reduced approximation is reasonable are defined as electroquasistatic [3]. This truncated version of Maxwell's equations [3] is

$$\nabla \times \mathbf{E} = -\frac{\partial}{\partial t}\mu_0\mathbf{H} \approx 0 \quad (2.9)$$

$$\nabla \times \mathbf{H} = \frac{\partial}{\partial t}\epsilon_0\mathbf{E} + \mathbf{J} \approx 0 \quad (2.10)$$

$$\nabla\epsilon_0\mathbf{E} = \rho \quad (2.11)$$

$$\nabla\mu_0\mathbf{H} = 0 \quad (2.12)$$

Where \mathbf{E} is the electric field intensity, \mathbf{H} is the magnetic field intensity, \mathbf{J} is the current density, μ_0 is the magnetic permeability of vacuum ($4\pi \times 10^{-7}$ N/A²) and ϵ_0 is the electric permittivity of vacuum (8.854×10^{-12} F/m). A given distribution of charge density ρ produces the electric field intensity \mathbf{E} ; the magnetic field intensity \mathbf{H} is approximated by zero. Note that the electric field \mathbf{E} , a vector quantity, is the gradient of the voltage V and is defined by [14]

$$\mathbf{E} = -\frac{dV}{dn} \quad (2.13)$$

Here n is the normal direction.

This electrostatic physics has been considered for the simulation by Electroquasistatic application mode that computes the electric energy stored in the total capacitive system.

2.4 Calculating Capacitance

A capacitor is characterized by its ratio of charge stored to applied voltage, called the capacitance and measured in Farads. Unlike a battery, when the voltage is removed, the capacitor discharges. The voltage V across a capacitor with charge Q and capacitance C is given by

$$V = \frac{Q}{C} \quad (2.14)$$

the potential energy stored in a capacitor is given by

$$W = \frac{CV^2}{2} \quad \Rightarrow \quad C = \frac{2W}{V^2} \quad (2.15)$$

Therefore, if the energy W is known the capacitance can be found, which can be compared with the estimations for the capacitance values calculated using the parallel plate approximation [27]. When a parallel-plate capacitor is filled with insulating material of dielectric constant ϵ_r , since the field is mostly confined to the space between the plates,

the dielectric will reduce \mathbf{E} and, hence, also the potential difference V , by a factor $1/\epsilon_r$. Accordingly the capacitance $C = Q/V$ is increased by a factor of the dielectric constant, $C = \epsilon_r C_{vac}$, where C_{vac} is the capacitance in vacuum. This is in fact a common way to enhance a capacitor.

If the capacitor is filled with a linear dielectric, its capacitance exceeds the vacuum value by a factor of the dielectric constant. Because part of the field is cancelled off by the bound charges, more free charges have to be pumped to achieve a given potential. It takes energy to charge up a capacitor, as Eqn. 2.15 shows. In case of a dielectric capacitor this energy is increased by the same factor ϵ_r .

For different values of energy stored it is possible to determine the values of capacitance for different states of relative humidity.

The capacitance C of a device depends upon the geometrical arrangement of its electrodes and the dielectric material employed between them. For a long planar, parallel-plate capacitor, the capacitance C is given [3] by

$$C = \epsilon_o \epsilon_r \frac{A}{d} \quad (2.16)$$

ϵ_r in this electrophysics has to be related with the mass or volume concentration in diffusion physics, in order to couple both physics together towards a multiphysics simulation.

2.5 Multiphysics

Both the physics of diffusion and electrostatics are coupled through a relationship between vapor mass or volume concentration and the permittivity of the polyimide at a certain time. When the sensor is exposed to an atmosphere with certain %RH, the sensor starts absorbing moisture. The mass concentration (Φ) inside the dielectric will change the mixed dielectric constant ($\epsilon_{r\text{mix}}$) with time due to Φ . As a result, capacitance or output signal of the sensor will change as $\epsilon_{r\text{mix}}$ changes. This is the basic principle describing how the present sensor works.

After an extensive search a concentration–permittivity relationship was found in a book [19] by Landau and Lifshitz. In their book an expression of the dielectric permittivity (ϵ_r) of an emulsion of low concentration was solved by integrating the local dielectric permittivity in the medium. With an arbitrary difference between ϵ_1 for the medium and ϵ_2 for the disperse phase, the value of combined ϵ_r resulted in

$$\epsilon_{r\text{mix}} = \epsilon_1 + \frac{3\phi\epsilon_1(\epsilon_2 - \epsilon_1)}{\epsilon_2 + 2\epsilon_1} \quad (2.17)$$

This formula is correct to terms of the first order in ϕ where ϕ is the volume concentration of the emulsion. This expression was found to be valid [19] only for a finely dispersed mixture such as an emulsion or powder mixture, etc. An attempt to apply this formula to the present multiphysics problem resulted in nonphysically high values of $\epsilon_{r\text{mix}}$.

At the very end of the present work at last a set of formulae was found in a nice study [15] done by Hartshorn et al. In accordance with their description, the dielectric constant of a mixture of two substances depends on the manner in which they are distributed throughout the material. If relative permittivities are ϵ_1 for the material and ϵ_2 for the water (or air) and $\epsilon_{r\text{mix}}$ for the mixture, the expressions for $\epsilon_{r\text{mix}}$ can be defined for three following cases:

- If the material and the water are in the form of layers parallel to the electrodes

$$\epsilon_{r\text{mix}} = \frac{1}{v_1\epsilon_1 + v_2\epsilon_2} \quad (2.18)$$

- When the layers are perpendicular to the electrodes

$$\epsilon_{r\text{mix}} = v_1\epsilon_1 + v_2\epsilon_2 \quad (2.19)$$

- For a random distribution of aggregates of the material in the mixture

$$\epsilon_{r\text{mix}} = \epsilon_1^{v_1} + \epsilon_2^{v_2} \quad (2.20)$$

Here, v_1 and v_2 stand for volume fractions V_1/V and V_2/V of the material and water (or air) respectively in the mixture. Here the second case would be applicable to the simulation of our work.

2.6 Microheater for Thermal Reset

As an addition to our work an embedded thermal heater is essential for a precise measurement by resetting. The absorption process tends to be faster than the desorption. Heat is required to produce a driving force in order to expedite desorption. In the working cycle of 1 s the absorbed moisture inside the polyimide dielectric layer has to be forced out to the surroundings. Thus the sensor can be reset for the next cycle. As the response time of the sensor is very short and the cycle time is 1 s only, this heater should work in a fraction of a second. The developed polysilicon heater will be occupying 1 mm² area on top of the Si-substrate with its own working area of $(902 \times 800) \times 10^{-12}$ m².

The wire thickness is kept at a value of 0.6 μm and width of 6 μm . A number of 56 coils is chosen, so that a total of 113 pieces of wires are joined together 2 μm apart from each other. Based on the electrical resistance of the coil material and input voltage

a certain amount of heat is generated. This generated power results in heat dissipation into the layers above the heater increasing the temperature of the layers to a prescribed temperature. The elevated temperature acts as a driving force to move the moisture off to the air. The simulation was performed in ANSYS by finite element method for the transient case with following governing heat diffusion equation (1 D)

$$\frac{\partial}{\partial y} \left(k \frac{\partial T}{\partial y} \right) = \rho C_p \frac{\partial T}{\partial t} \quad (2.21)$$

Here, T is the temperature, ρ and C_p are the density and heat capacity of the conductive material respectively. k is the thermal conductivity of the material.

If the entire domain of materials is considered to be thermally conductive, the governing transient energy equation [17] by lumped capacitance method can be written as

$$\frac{P}{A} - h(T_s - T_\infty) = \rho L C_p \frac{\partial T}{\partial t} \quad (2.22)$$

Here, P is the thermal energy generated by ohmic effect, A is the area, h , convection coefficient, T_s , surface temperature and T_∞ is the ambient temperature.

The time dependent result for various values of heat flux (see Figure B.1 in Appendix B) shows that a high surface temperature can easily be obtained in a small fraction of one second. If shorter response times are required this power could be increased, or vice versa. The simulation was performed with ANSYS simulator to study the effect of different heat fluxes on the surface temperature T_s . The encouraging results of this simulation indicate that the design of the microheater for thermal reset would not present a major problem in the pursuit of measurement cycles of less than one second. Therefore, the remaining of this study will concentrate on the capacitive sensor.

The step by step discussions found in above sections lead us to start previewing the sensor development in following chapters.

Chapter 3

Simulation/Modeling

In the beginning of the this chapter, the terms ‘response time’ and ‘integrated water vapor mass’ should be introduced.

3.0.1 Response Time

Response time is the most important design parameter in the present study. In order to compare different sensor designs, a clear definition of response time is required. The difficulty in defining the time for a sensor response is caused by the asymptotic approach of the sensor to a new steady-state. The time to reach the steady-state value can be long and depends on the accuracy used, because the change in signal in the final stages is very small. To overcome this difficulty, the response time is defined as the time for the output signal to reach 90% of the change towards a new steady-state. For example, if the system has an initial output signal of zero at $t = 0$, the response time is the time taken for the output signal to reach 90% of the final value.

3.0.2 Integrated Water Vapor Mass

The second most important parameter used to compare different sensor designs is the total amount of water vapor mass absorbed by the dielectric, in particular, inside the Effective Domain (for definition, see section 3.5) between the electrodes. The strength of the output signal is expected to be proportional to this quantity. Along with some modifications the FEMLAB simulator is able to calculate the amount of integrated mass in specific subdomains at different time steps.

3.1 Description of the Sensor

The sensor being developed is a capacitive device and is expected to satisfy the requirements of high linearity and wide range of dimensions from a few centimeters to a few micrometers. The basic sensing element of a capacitive device consists of two electrodes with capacitance C , where

$$C = f\{\varepsilon\} \quad (3.1)$$

i.e. if distance (d) between two electrodes and area (A) of the electrodes are kept constant, C is a function of the permittivity (ε) of the dielectric. In addition, for a moisture absorbing dielectric material, ε is a function of moisture content (M) and temperature (T). Therefore,

$$\varepsilon = f(M, T) \quad (3.2)$$

This introduces a so-called Variable Dielectric Displacement Method [38] by which a linear relationship between dielectric constant and capacitance can be obtained.

3.1.1 Thin layers and dimensions

With an overall size of 1 mm^2 the geometry of this model (see Figure 3.1) consists of many interdigitated metallic fingers (gold) immersed in a thin polyimide dielectric layer. More than hundred interdigitated fingers, all connected in parallel, play the role of electrodes. A $0.5 \text{ }\mu\text{m}$ LTO (low thermal oxide) layer as an electrical insulator [18] is deposited between the dielectric layer and the structure of electrodes. A 200 nm thick Si_3N_4 layer is deposited just above the substrate to act as a thermal insulator to the polysilicon heater. The coils of a polysilicon heater placed just underneath the sensor are insulated by a $0.5 \text{ }\mu\text{m}$ LTO layer as well.

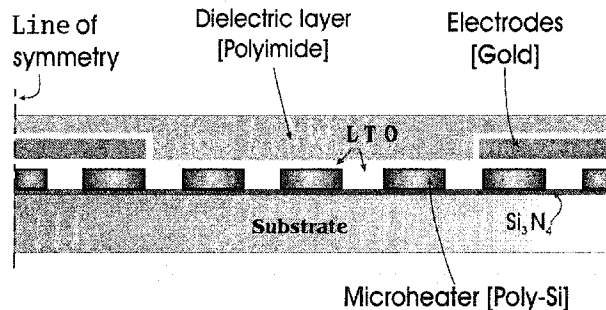


Figure 3.1: A 2D symmetric view of the system.

3.1.2 Materials and properties

A faster curing and faster imidizing polyimide (PI2556 – HD MicroSystems) is selected as moisture sensing dielectric material for this study. The cured film of PI2556 has a tensile modulus of 2.45 GPa , a moisture uptake of 3% at $100\% \text{ RH}$, a coefficient of thermal expansion of $40 \text{ ppm}/^\circ\text{C}$ at 300°C . The saturation concentration of water vapor in this polyimide at ambient temperature is $49 \text{ kg}/\text{m}^3$. It has a dielectric constant of 3.3 at 1 kHz , with a breakdown voltage of $4 \text{ V}/\mu\text{m}$. A list of properties for materials used in the simulation is given in Table A.2. In particular, the selected polyimide offered maximum moisture uptake, allowing at the same time a small film thickness.

This particular polyimide was chosen after a thorough selection process [22, 20, 18]. The major factors influencing the selection process were moisture uptake, film thickness, dielectric constant, glass transition temperature, etc. Some factors relating to micromachining were coefficient of thermal expansion, cure temperature, imidizing speed, adhesiveness to substrate, good processability, coating method, etc. A list of some polyimides [16] that were considered in the selection is given in the Appendix A in table A.3. This table can be helpful to analyze different properties of a series of polyimides.

3.2 FEMLAB and MATLAB: simulation software

FEMLAB is a powerful engineering tool for modeling and solving scientific and engineering problems based on finite element methods (FEM) solution of partial differential equations. It is well suited for state-of-the-art multiphysics modeling, such as MEMS. It can either work in Matlab interactive environment or in its own platform. It is possible to harness its power either through a flexible graphical interface of its own or from the Matlab prompt.

Two application modes, 'Diffusion' and 'Electrostatics' from the Engineering module and Electromagnetic module respectively, are used in the simulations for this work. The diffusion equation is modeled in the Diffusion mode where diffusion coefficient, D , describes the diffusivity of the material. During the entire simulation a value of D is assigned to each domain, considered to be an isotropic material. As explained in section 2.3, a modified version of Maxwell's equations is considered in the simulation where this specific application mode is termed as electroquasistatic. In electrostatics, the scalar electrostatic potential is related to the electric field density, whereas this electric field density depends on the relative permittivity, ϵ_r , of the material. It is assumed that the concerned materials are all isotropic showing individual scalar value of ϵ_r for each of them.

In FEMLAB, subdomain integration for mass concentration and electric energy in a certain subdomain could be calculated in the post mode environment. In Matlab workspace a function called 'fspline' helped to calculate the response time according to the definition explained in section 3.0.1. For the calculation of capacitance Eqn. 2.15 was used with the value of integrated electrical energy (W) obtained in FEMLAB.

In FEMLAB the integrated mass and electrical energy could be performed only for a specific time step at a time. But for the ease of simulation and post-processing calculations, integrated values of these variables for all time steps were to be obtained and stored in a single vector. For these purposes the 'fem' data structure from FEMLAB had to be exported (with mesh and solution) to the Matlab workspace and some modifications were done in the workspace. A part of the Matlab coded 'fem' structure along with the modifications for the present project is given in Appendix C.

In the following sections the simulation domain is explained together with boundary conditions and assumptions being applied.

3.3 Simulation Domain

Taking advantage of the symmetries of the sensor design, a two dimensional approach is used to simulate a single section of the interdigitated capacitor, as shown in Figure 3.2. This single section is composed of half section of each of two consecutive electrodes with a full dielectric section between them.

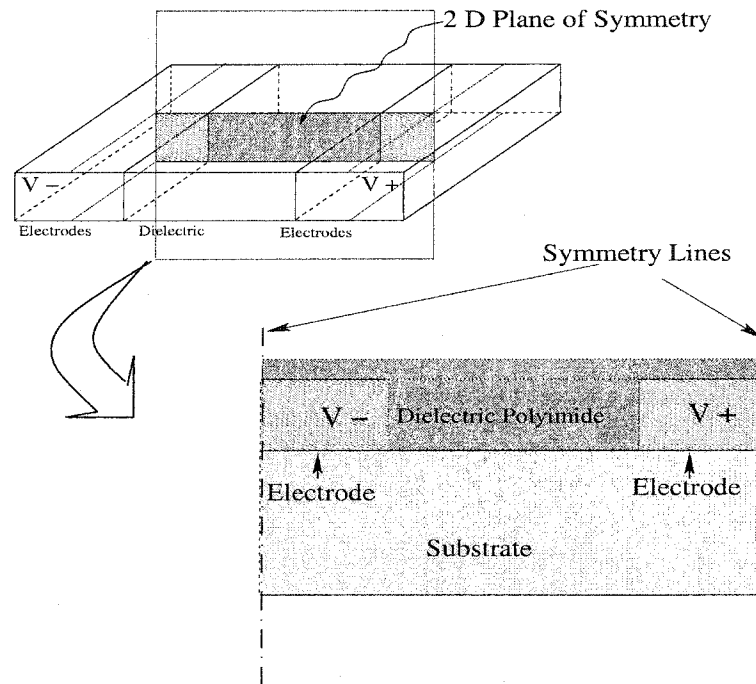


Figure 3.2: Approach on 2D domain.

3.4 Assumptions

The simplified computational domain uses the following assumptions:

- The domain has a unitary width.
- The effects of the ends of the electrodes can be neglected because we assume comparatively long electrodes.
- The value of mixed dielectric constant, $\epsilon_{r_{mix}}$ is assumed constant at an average value of 42.

- Materials are assumed isotropic.
- No swelling effect.
- Working temperature is uniform at a nominal constant value.
- Air subdomain height over the sensor is infinitely long.

3.5 Simulation Model

Capacitive sensors electronically measure the capacitance between two or more conductors in a dielectric environment, usually air or a liquid. A similar technique is electric field measurement, where the electrostatic voltage field produced by conductors in a dielectric environment is picked by a probe and high impedance amplifier [35].

As stated in the previous section, the capacitance measured by the sensor is proportional to the moisture content in the polyimide layer. The two-dimensional water vapor diffusion into polyimide is expressed as:

$$\frac{\partial \Phi}{\partial t} = D \left(\frac{\partial^2 \Phi}{\partial x^2} + \frac{\partial^2 \Phi}{\partial y^2} \right) \quad (3.3)$$

Here D is the diffusion coefficient, Φ the concentration of the diffusing species (water vapor) and x, y the diffusion axes.

For the calculation of time dependent moisture concentration and integrated total mass of water vapor, a two-dimensional section of the periodically occurring space between two electrode centers is used, as shown in Figure 3.3 (top). The air limits the domain on the top and is considered an infinite source at constant humidity.

The initial and boundary conditions, as well as properties are as follows:

$$\begin{aligned} \Phi_{substrate} &= \Phi_{electrodes} = 0 \\ \Phi_{polyimide} &= 0 \\ \Phi_{air} &= 46.6 \text{ kg/m}^3 \\ D_{substrate} &= D_{electrodes} = 0 \\ D_{polyimide} &= 5 \times 10^{-13} \text{ m}^2/\text{s} \end{aligned}$$

Two types of subdomains of polyimide are taken into consideration for the investigation of water vapor diffusion into the polyimide. One is the whole domain consisting of polyimide, called *Total Subdomain*, and the other, called *Effective Subdomain*, corresponds to the polyimide that lies in between the two electrodes only (Figure 3.3, bottom). The importance behind defining the effective domain is that it stands for the dielectric region between two electrodes. Monitoring of this region in the simulation is important to predict the accurate response of the sensor.

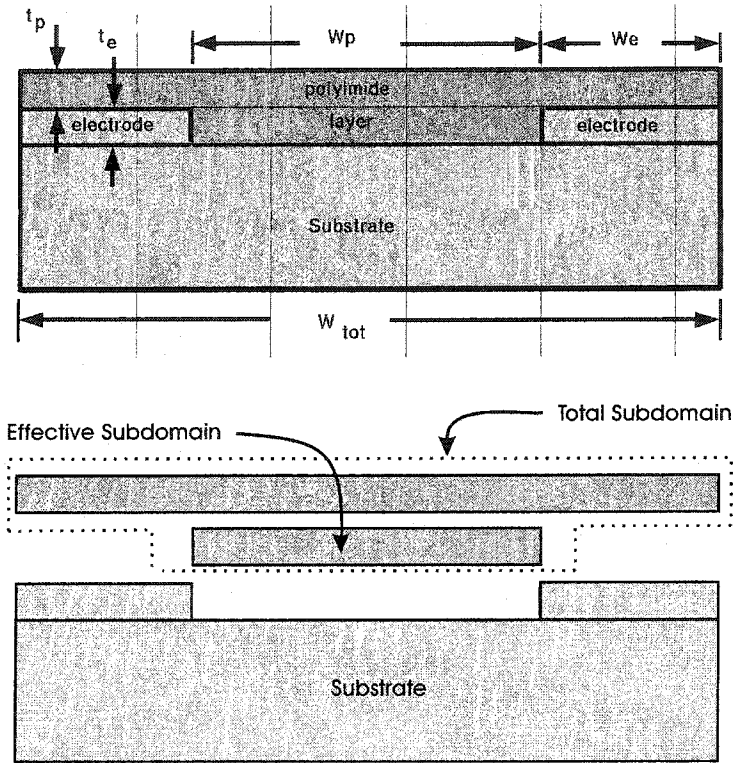


Figure 3.3: Total and Effective Subdomains.

3.6 Boundary Conditions and Multiphysics

3.6.1 Dirichlet and Neumann

Figure 3.4 and Figure 3.5 show the boundary conditions applied in both diffusion and electrostatics modes. A Dirichlet boundary condition is given to those boundaries where values are prescribed. For continuous or insulation as well as symmetry or impervious boundaries a special type of Neumann boundary condition is applied.

Diffusion Model

To avoid false numerical diffusion across the interface between absorbent and non absorbent materials only total subdomain and air domain are set active at the time of this simulation. The surroundings of air subdomain are assigned to a prescribed value of relative humidity corresponding to an infinite source of water vapor. The top surface of the inactive domain is assigned to have zero concentration gradient, since this is an impervious surface (see Figure 3.4).

There is no boundary condition applied to the top surface of the polyimide layer. It is an interface between the polyimide and air domains. As the moisture diffusion coeffi-

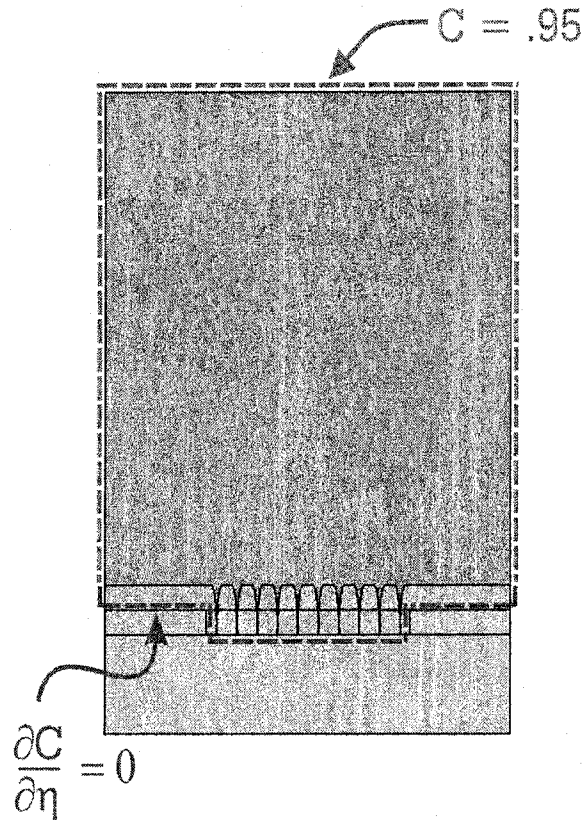


Figure 3.4: Boundary conditions applied in Diffusion mode.

coefficient in air ($D_{air} = 2.5 \cdot 10^{-5} \text{ m}^2/\text{s}$) [11] is several orders of magnitude higher than that in polyimide ($D_{polyimide} = 5 \cdot 10^{-13} \text{ m}^2/\text{s}$) [18, 20], it is reasonable physically to neglect the concentration drop inside of air domain. A Neumann boundary condition is given to the boundaries, which correspond to symmetry planes. The bottom surface of the polyimide domain is provided with impervious boundary condition which represents no flux across this interface.

Initial values are given to the air domain having a moisture diffusion coefficient of $2.5 \cdot 10^{-5} \text{ m}^2/\text{s}$ and that for polyimide region equals $D_{polyimide}$ (see section 3.5 in page 24).

Electrostatic Model

For the electrostatic simulation an applied voltage (V) is given around one of the electrodes and ground ($V = 0$) for the other. Outside borders of the whole domain are set to Neumann boundary condition (see Figure 3.5). The symmetry lines at the electrodes are provided with Dirichlet boundary condition. They could also be set to Neumann, but Dirichlet is better here for convergence.

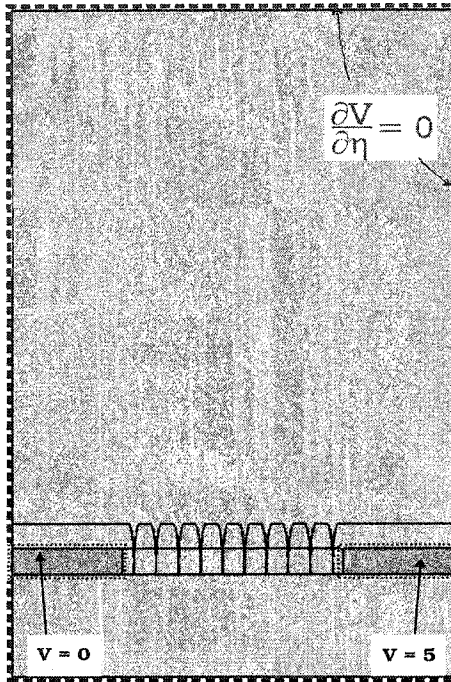


Figure 3.5: Boundary conditions applied in Electrostatic mode.

3.6.2 Multiphysics

Due to time constraints and difficulties related with the implementation of multiphysics in FEMLAB, an average constant value of mixed dielectric constant ($\epsilon_{r\text{mix}} = 42$) was used in the present study, and no multiphysics calculation was performed.

Chapter 4

Parameter Study

A comprehensive parameter study of the humidity sensor design is done and it is divided into two perspectives:

1. Diffusion Perspective
 - (a) Surface Geometry: concerns the air contact surface of the polyimide layer.
 - (b) Domain Geometry: concerns the thickness and width of the 2D subdomains.
2. Electrostatic Perspective
 - (a) Air Domain: concerns an air domain above the polyimide film.
 - (b) Domain Geometry: concerns thickness and width of the 2D subdomains.

4.1 Diffusion

The diffusion perspective emphasizes the fact that to minimize sensor response time, it is necessary that the effective subdomain absorbs the maximum amount of water vapor in a very short span of time. The goal is for the response time in this diffusion process to be near .5 s to achieve the final sensor measurement cycle of less than 1 s.

In diffusion process four parameters are involved which should be studied to find out the shortest response time:

1. Diffusion coefficient of the dielectric material. Once the dielectric material is selected to be a polyimide, the value of D can vary only within the limits of available polyimides at this stage.
2. Height of the subdomains involved in diffusion.
3. Distance of the dielectric region between two electrodes (width of effective subdomain).
4. Air contact surface of the polyimide.

4.1.1 Diffusion Coefficient, D

The highest possible diffusion coefficient should be selected, since the response time can be reduced with a higher diffusion coefficient. To find a polyimide with a higher D , a thorough search was done on studies using polyimides [22, 20, 18] and on the polyimides available in the market. This search indicated that cross-linked Pyralin would be an appropriate polyimide type for the present sensor. For a long time the PI2555 series Pyralin has proved to be a suitable moisture sensitive polyimide, according to the manufacturer, HD Microsystems [5]. Moisture absorption of PI2556 at saturation (100% RH) is over 3.5%. PI2556 is strongly recommended [5] and was thus purchased for this project to be dispensed over the MEMS structure with a desired thickness. For simulations, the diffusivity value used was $5 \cdot 10^{-13} \text{ m}^2/\text{s}$ [18, 20] for water vapor in polyimide.

4.1.2 Height of the Subdomains

Height of the total subdomain comprises the thickness of polyimide film above electrodes and the thickness of electrodes. This electrode thickness is the height of effective subdomain as well (see Figure 4.1).

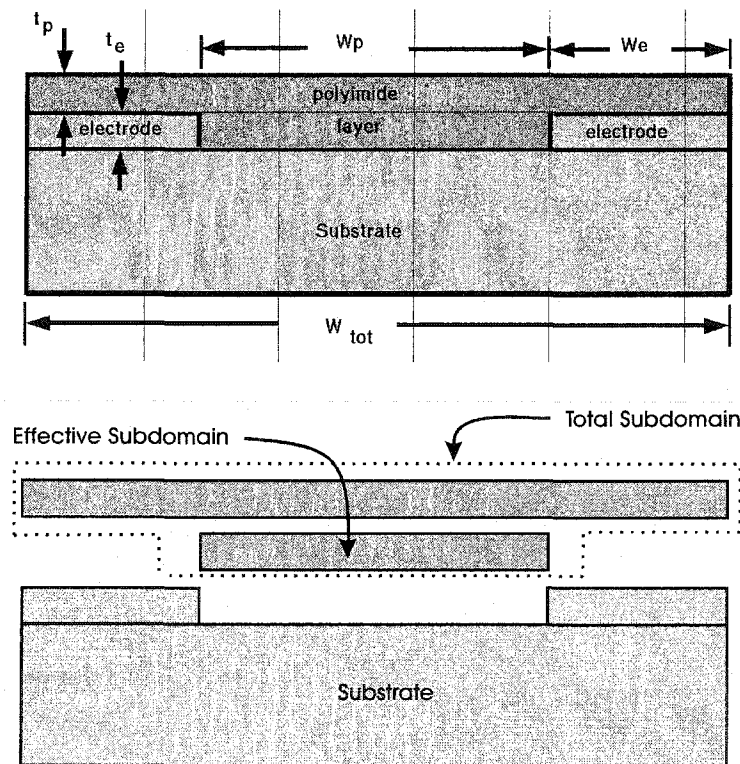


Figure 4.1: Dimensions of the subdomains.

4.1.3 Width of the Effective Subdomain

The effective subdomain has a width which is in fact the distance of the dielectric region in between two electrodes (see Figure 4.1).

4.1.4 Air Contact Surface of the Polyimide

Air contact surface of the sensor is one of the vital parts of this parameter study. Since the diffusive flux is proportional to the surface area, a significant increase in this area can shorten the response time dramatically.

In the diffusion perspective, air contact surfaces and dimensions of the 2D domain are studied thoroughly following two different stages:

- Surface Geometry
- Domain Geometry

4.2 Electrostatics

In case of the electrostatics perspective the output signal, whether in voltage or frequency, has to be stronger with less noise. For an efficient simulation, the extent of the region dominated by electrostatic field should be determined and then optimized ensuring less computational time. To achieve the design goals a comprehensive study on the dimensions of both 2D polyimide domain and the air domain was performed.

4.3 Diffusion: Parameter Study

4.3.1 Surface Geometry

Ten different shapes of the polyimide surface (Figure 4.2) are considered in search of an optimized response time of diffused mass of water vapor, which is directly related to the capacitance. An example of results of water vapor diffusion over time into the effective domain is shown in Figure 4.3. The steady state levels of integrated total mass absorbed allow for the comparison of response levels of various shapes. Figure 4.4 shows the 2D view diffusion solution in model Dim4.

The air contact polyimide surface of Dim1 bears the simplest shape. This surface is totally flat having minimum amount of area exposed to humid air. As the rate of water vapor accumulation inside polyimide depends on the extent of this area and time to reach steady-state depends on the depth of total subdomain, this model is expected not to be very sensitive. However, Dim1 is taken into account throughout the study as the standard shape. Dim2 is designed to be a surface having a rectangular groove in the upper

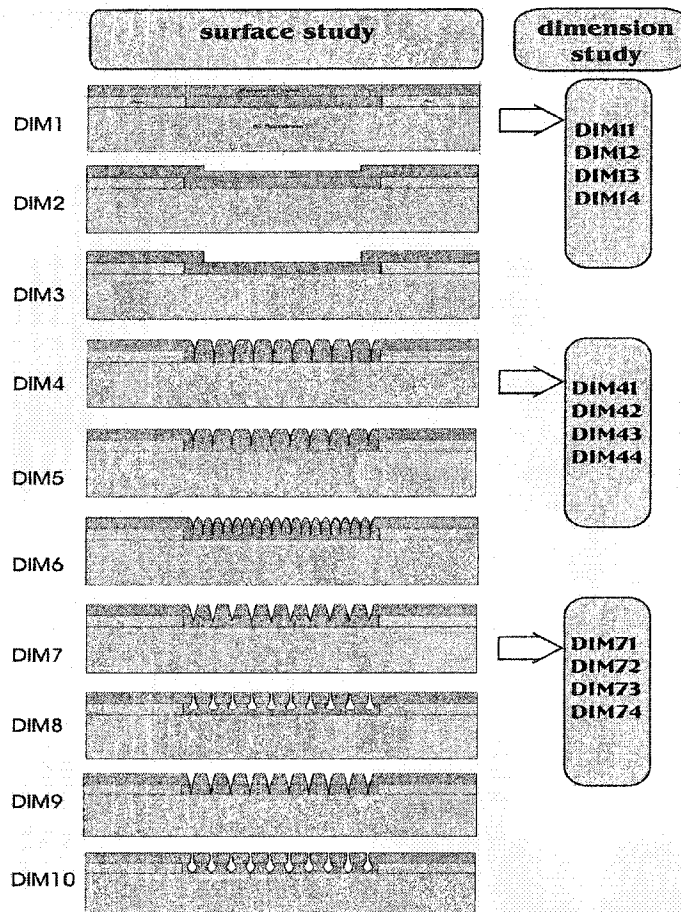


Figure 4.2: Different shapes and dimensions used in the parameter study.

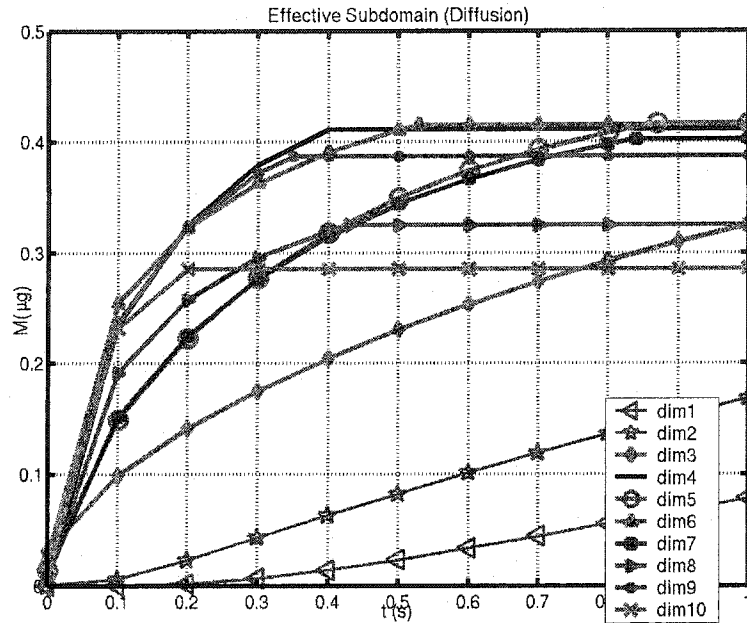


Figure 4.3: Water vapor accumulation in effective subdomain over time.

polyimide layer. The height of the total subdomain is decreased and the surface area is increased slightly, but the rate of water vapor accumulation is still not appreciable. A slight change in Dim2 introduces Dim3, which has an important feature. Here the depth of the total subdomain is decreased to an extent to let the top surface of effective subdomain exposed to air. It shows a clearly shorter response time than those of Dim1 and Dim2, and the amount of water vapor accumulated in the effective subdomain is satisfactory. However, for all these three models the diffusion process does not reach a steady state condition even in 10 s.

A concept to allow the humid air a more direct access into the effective domain is introduced in Dim4, and it shows excellent results both in response time and water vapor accumulation. Dome-shaped surfaces are introduced in this design, and the surface resembles polyimide columns of dome-shaped top between the pairs of electrodes. Dim5 is an approach slightly modified from Dim4. Here the air gap between two columns is not as deep as in case of Dim4. As a result of this, the amount of water vapor accumulation is almost same but the rate is much slower than Dim4. Dim4 and Dim6 behave in a similar fashion, but in case of Dim6, increase in number of columns does not increase the amount of water vapor accumulation at steady state. Increase in number of columns would lead to narrower columns, which may also pose problems during micromachining. Dim7 and Dim8 both have different types of shapes. Although both show satisfactory results for both moisture accumulation and response time, they actually contain an undesired design

Time=2 Surface: concentration (c)
Arrow: [electric field (Ex),electric field (Ey)]

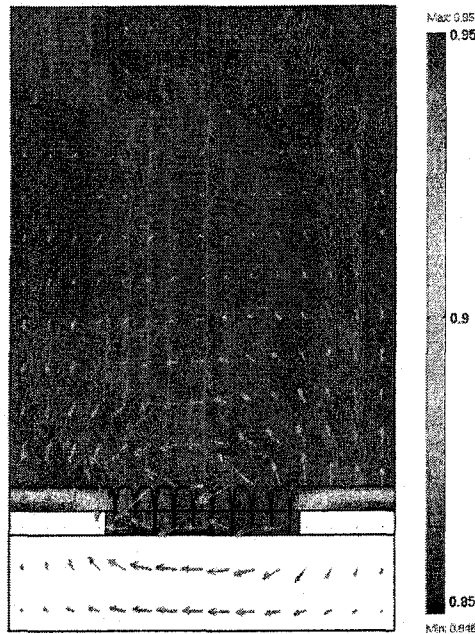


Figure 4.4: 2D view of diffusion solution and electric field in Dim4 at steady state.

feature where the effective domain does have a significant portion of its volume with no polyimide but with air. This undesired design would result in comparatively lower electrical energy. Finally, Dim9 and Dim10 are the extended versions of Dim7 and Dim8, respectively, and both are disregarded for the same reason.

From this point on, Dim9 and Dim10 are removed from this study as Dim7 and Dim8 are sufficient to represent them. This is because Dim9 shows that it can respond within .3 s, but the mass content does not reach what is expected. In addition, the bulk amount of no-polyimide area inside the effective domain in Dim9 can decrease the signal significantly. On the other hand, Dim10 shows a shorter response time, but here Dim10 is also disregarded for the same reason (large no-polyimide region).

From Dim4 to Dim8 the results from the parameter study of surface show that the value of total mass of water vapor in the **total subdomain** varies between $1.095 \mu\text{g}$ and $1.186 \mu\text{g}$, showing that Dim4 in this study is carrying a $1.164 \mu\text{g}$ of water vapor with the shortest response time at steady state. It should be mentioned that the steady state of mass accumulation in the effective subdomain is important to the simulation.

Because the simulation is being based on the principle of a capacitor, the effective domain here should be the main domain of interest considering that the electrical field

Table 4.1: Results: Dim4 to Dim8 at steady state.

M – total mass of water (μg), T_r – response time (s)

Model	M	T_r
Dim4	.411	.40
Dim5	.416	.87
Dim6	.415	.53
Dim7	.402	.84
Dim8	.325	.43

is essentially confined in this subdomain [14]. As a result a significant change in ϵ_r will be caused by a significant amount of water accumulation in the effective domain. This means that the effective subdomain will contribute most to the change in capacitance and consequently to the output signal.

In Figure 4.3 from Dim4 to Dim8 it is shown that in the **effective subdomain**, the value of total mass of water vapor varies between $.325 \mu\text{g}$ and $.416 \mu\text{g}$ for different cases, showing that Dim4, Dim5 and Dim6 carry almost the same amount of water when they reach a steady state condition. But the response time for Dim4 is .40 s. It is the shortest response time and corresponds to a water vapor mass of $.411 \mu\text{g}$ (see Table 4.1). Though Dim5 and Dim6 have the water accumulation of $.416 \mu\text{g}$ and $.415 \mu\text{g}$, respectively, they are not as responsive as Dim4. Hence the surface shape of Dim4 is chosen to satisfy the purpose of the parameter study in the diffusion perspective.

Of all other surface geometries, Dim7 and Dim8 are special cases that accumulate about $.402 \mu\text{g}$ and $.325 \mu\text{g}$ of water vapor, respectively, in effective subdomain. Dim7 has a response time of .84 s and Dim8 of .43 s.

4.3.2 Domain Geometry

After studying water vapor accumulation rate and amount of absorbed mass, it is clear so far that Dim4 is the most efficient shape. In addition, Dim1 was chosen as a standard design for comparison. Now, for this parameter study both Dim1 and Dim4 are considered. So, further study on domain geometry is performed on Dim1 and Dim4 (Figure 4.2).

The results from the domain geometry study, namely total mass M and response time T_r , for various combinations of the domain dimensions are shown in Table 4.2 (based on effective subdomain, see Figure 4.1). This study, where width of the effective subdomain W_p is kept $10 \mu\text{m}$, demonstrates clearly that a considerable decrease in the thickness (t_p) of the upper layer of polyimide and an increase in the height of electrodes (t_e), which

Table 4.2: Results: Domain geometry study on Dim4 for diffusion.

W_e – width of electrodes (μm), W_{tot} – total width of the domain (μm), t_e – height of the electrodes (μm), t_p – height of the upper polyimide layer (μm), M – total mass of water (μg), T_r – response time (s)

Dim	W_e	W_{tot}	t_e	t_p	M	T_r
Dim41	5.0	20	1.0	1.00	.41	.40
Dim42	5.0	20	1.0	0.50	.41	.37
Dim43	5.0	20	1.5	0.50	.62	.39
Dim44	5.0	20	2.0	0.50	.82	.39

Table 4.3: Results: Domain geometry study on Dim1 for diffusion.

W_e – width of electrodes (μm), W_{tot} – total width of the domain (μm), t_e – height of the electrodes (μm), t_p – height of the upper polyimide layer (μm), M – total mass of water (μg), T – simulation time (s)

Dim	W_e	W_{tot}	t_e	t_p	M	T
Dim11	5.0	20	1.0	1.00	.08	2
Dim12	5.0	20	1.0	0.50	.09	2
Dim13	5.0	20	1.5	0.50	.18	2
Dim14	5.0	20	2.0	0.50	.31	2

corresponds to the depth of the effective subdomain, would lead to an acceptable response time. As a result Dim42 shows response time of .37 s which is the shortest, Dim41, Dim43 and Dim44 show similar response times of .4 s, .39 s and .39 s, respectively.

The amount of water vapor mass in the effective subdomain of each in Dim4 (see Table 4.2) is acceptable and shows large improvement over each in the reference case Dim1 (see Table 4.3) after an absorption time of 2 s. The total mass of water vapor in effective subdomain increases proportionally with the height of this subdomain (t_e).

4.4 Electrostatic: Parameter Study

4.4.1 Air Subdomain

In 2D model it was necessary to attach to the surface of polyimide an air subdomain through which the electric field would pass, as it would in reality. Therefore, an additional subdomain is introduced at the top of the polyimide surface (see Figure 4.5) and this will be acting as humidified air surroundings. The properties of air at 35°C and 1 atm being

used in this subdomain are given in Table 4.4.

Table 4.4: Air properties used.

Properties of Air	
Density, ρ	1.1314 kg/m ³
Dielectric constant, ϵ_r	1 [assumed to be vacuum]
Vapor diffusion coefficient in air, D	2.5×10^{-5} m ² /s [11]

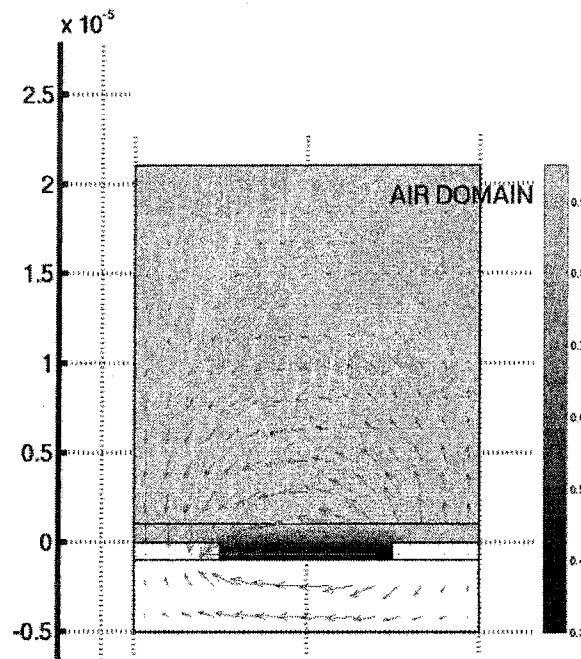


Figure 4.5: System with air subdomain. Arrows indicate the electric field.

A supplemental numerical study [2] was done to find out the optimum finite thickness of the air subdomain to ensure that the electric field is confined in this domain. This will justify the assumption of the domain being infinitely long along its height, which is required for the application of Neumann type boundary condition, as described in section 3.6. From Figure 4.7 it can be concluded that for the specific designs involved in this project a thickness of around 20 μm for the air subdomain can serve the simulation purpose satisfactorily.

4.4.2 Domain Geometry

By adding a sufficiently long air subdomain the 2D simulation model is correctly set up to work with the electrostatic mode. Now a complete study on the dimensions of model

Time=2 Surface: electric potential (V)

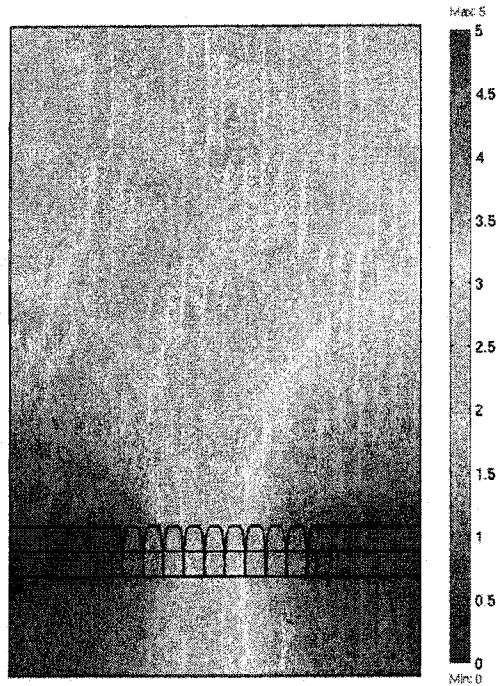


Figure 4.6: Surface diagram of Electric Potential in the system of Dim4.

Table 4.5: Results: Domain geometry study on Dim4 for electrostatics.

W_e – width of electrodes (μm), W_{tot} – total width of the domain (μm), t_e – height of the electrodes (μm), t_p – height of the upper polyimide layer (μm), C – Capacitance (pF)

Dim	W_e	W_{tot}	t_e	t_p	C
Dim41	5.0	20	1.0	1.00	21
Dim42	5.0	20	1.0	0.50	20
Dim43	5.0	20	1.5	0.50	31
Dim44	5.0	20	2.0	0.50	42

geometry will help to explore the pattern of output signal as well as the optimized shape of the MEMS structure. This being a 2D simulation the values for the electrical energy and capacitance calculated are all per unit length.

A preliminary electrostatic simulation is performed on the same geometries used in the previous domain geometry analysis in the diffusion perspective on Dim4 (see section 4.3.2 in page 34). The results in Table 4.5 show that a decrease in upper polyimide height decreases the capacitance slightly, whereas an increase in electrode height consid-

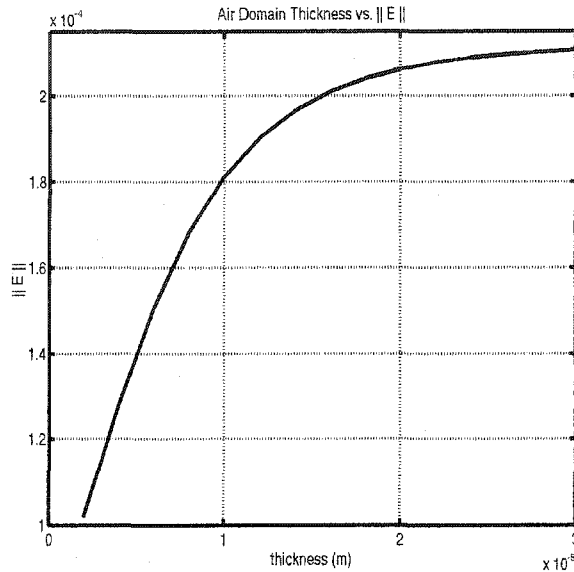


Figure 4.7: Total electric field as a function of thickness of the air subdomain.

erably increases the capacitance and, thus, the output signal.

The electrostatic parametric study on domain geometry is divided into three types of parameter variation:

- varying dielectric width (W_p)
- varying electrode height (t_e)
- varying electrode width (W_e) keeping minimum W_p

Because of substantial reduction in computing time, the standard model Dim1 is used for the simulation in this electrostatic parameter study. The conclusions from the study are expected to apply to a geometry based on Dim4 as well.

4.4.3 Varying Dielectric Width (W_p)

This study compares four types of W_p for constant electrode width (W_e) and electrode height (t_e) where $W_e = 5 \mu\text{m}$ and $t_e = 1.5 \mu\text{m}$:

1. Model0: $W_p = 2 \mu\text{m}$
2. Model1: $W_p = 5 \mu\text{m}$
3. Model2: $W_p = 7 \mu\text{m}$
4. Model3: $W_p = 10 \mu\text{m}$

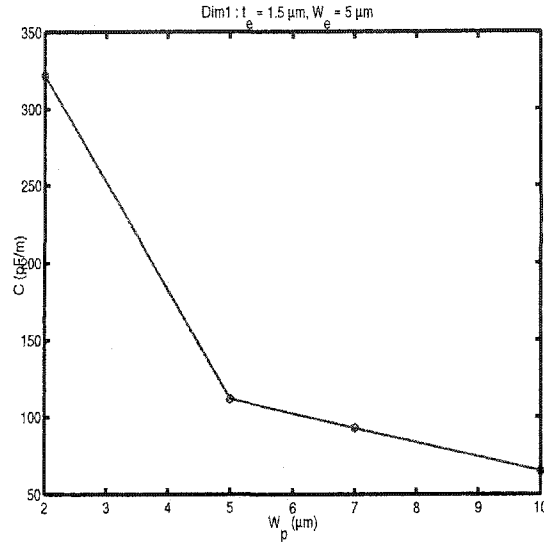


Figure 4.8: Capacitance against dielectric width.

Results in this simulation (with Model Dim1) for diffusion of water vapor inside polyimide are given in Table 4.6 (Capacitance is calculated with applied voltage, $V = 5$ V with an assumption that $\epsilon_{r\text{mix}} = 42$). The same results can also be seen in Figure 4.8, showing the behavior of the capacitance over changes in dielectric width.

Table 4.6: Results: Varying W_p on Dim1.

W_p – dielectric width (μm), M – water vapor mass content (μg), W – electrical energy (J), C – capacitance (pF)

Model	W_p	M	$W \times 10^{10}$	C
Model0	2	.164	40.25	322
Model1	5	.319	13.97	112
Model2	7	.423	11.60	93
Model3	10	.579	8.13	65

Table 4.6 reveals some important points as follows:

- With $W_p = 2 \mu\text{m}$, the value of capacitance is 188% larger than that in case of the model with $W_p = 5 \mu\text{m}$.
- In contrast, mass content in model0 ($W_p = 2 \mu\text{m}$) is about 50% less than that in model1 ($W_p = 5 \mu\text{m}$), which may not be desirable.

- On the other hand in both model2 and model3, though the mass content increases by 30% to 80% from model1, values of capacitance fall down.
- Theoretically, as considerable amount of mass would affect the electric field in the dielectric region, it would significantly change the dielectric constant of polyimide. As a result a stronger output signal can be expected. But a question arises whether the larger distance between two electrodes leading to weaker electrical energy might cancel this effect. It is important to bear in mind that very sensitive output signals would not be good for measurement. Rather a compensation could be made to the electrical energy by increasing the applied voltage if the electric signal becomes too weak.
- Finally, a channel with 2 μm width may not be suitable for an appropriate micro-fabrication [39].

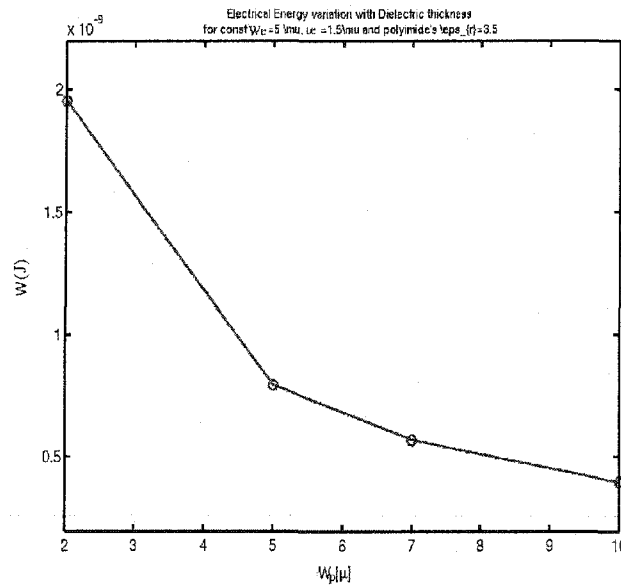


Figure 4.9: Electrical energy variation for different dielectric width.

The change in electrical energy (W) with the dielectric width (W_p) for a fixed electrode height is shown in Figure 4.9. A reduction in W_p corresponds to a large increase in electrical energy. In addition, for a fixed size capacitive humidity sensor, the smaller the dielectric width the larger the number of fingers in the interdigitated structure, which again improves the total electrical energy.

On the other hand, if the width of dielectric is kept on increasing beyond 10 μm , W_e will no longer decrease considerably as it does while W_p is being increased from 2 μm to 10 μm . As 2 μm is not recommended for microfabrication [39] this width is ignored,

and dielectric widths (W_p) of $5 \mu\text{m}$ and $10 \mu\text{m}$ should be checked in practice as test specimens.

4.4.4 Varying Electrode Height (t_e)

The height of the electrodes is tested for two different sizes of dielectric width, W_p in order to determine whether the effective dielectric area involved in the 2D analysis really matters in case of electrical energy and also to which extent.

For both cases the electrode width, W_e is kept $5 \mu\text{m}$ in size and the electrostatic analysis is also performed considering $\epsilon_{r\text{mix}}$ constant at 42 and with applied voltage $V = 5 \text{ V}$ as before.

Dielectric width (W_p) of $10 \mu\text{m}$

Three models are involved here:

1. Model4: $t_e = 0.5 \mu\text{m}$
2. Model5: $t_e = 1.0 \mu\text{m}$
3. Model6: $t_e = 1.5 \mu\text{m}$

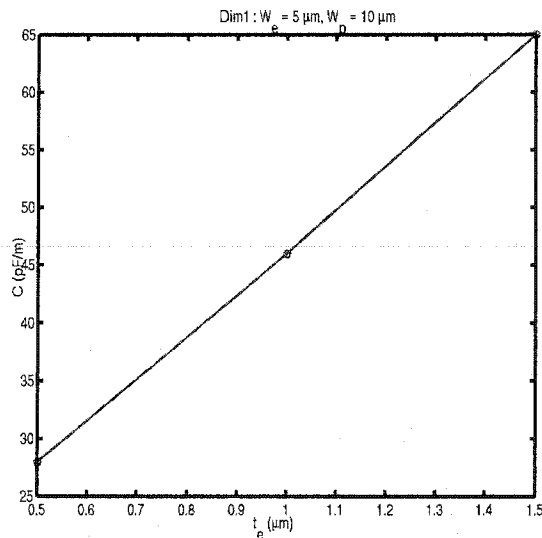


Figure 4.10: Capacitance against electrode height.

From Figure 4.10 it is seen that the concerned relationship here is almost linear. Results obtained are listed in Table 4.7. An increase in t_e from $.5 \mu\text{m}$ to $1.0 \mu\text{m}$ increases the mass content and also the value of capacitance. A further increase in t_e from $1 \mu\text{m}$

Table 4.7: Results: Varying t_e on Dim1 with $W_p = 10 \mu\text{m}$.
 t_e – electrode height (μm), M – mass content (μg), W – electrical energy (J), C – capacitance (pF)

Model	t_e	M	$W \times 10^{10}$	C
Model4	0.5	.404	3.49	28
Model5	1.0	.544	5.81	46
Model6	1.5	.579	8.13	65

to $1.5 \mu\text{m}$, though it increases C , it does not seem to affect M much. In section 4.3.2 in Table 4.2, it was already found that an increase in t_e from $1 \mu\text{m}$ to $1.5 \mu\text{m}$ did not change the response time. In addition, increases in electrode height cause significant increase in manufacturing costs. This analysis indicates that we should limit the electrode height (t_e) not to exceed the dimension of $1.5 \mu\text{m}$.

Dielectric width (W_p) of $5 \mu\text{m}$

Three models are involved here:

1. Model7: $t_e = 0.5 \mu\text{m}$
2. Model8: $t_e = 1.0 \mu\text{m}$
3. Model9: $t_e = 1.5 \mu\text{m}$

Table 4.8: Results: Varying t_e on Dim1 with $W_p = 5 \mu\text{m}$.
 t_e – electrode height (μm), M – mass content (μg), W – electrical energy (J), C – capacitance (pF)

Model	t_e	M	$W \times 10^{10}$	C
Model7	0.5	.231	6.92	55
Model8	1.0	.302	11.57	93
Model9	1.5	.319	13.97	112

Obtained results are listed in Table 4.8 and the conclusions are as follows:

- The amount of mass absorbed with electrode height of $1.5 \mu\text{m}$ is almost the same as that for $1 \mu\text{m}$.
- But the electrical energy and capacitance, for the entire sensor would be twice as much with $W_p = 5 \mu\text{m}$ as it is in the case of $W_p = 10 \mu\text{m}$, as shown in the tables (see Table 4.7 and Table 4.8).

All the above energy study was performed for a constant mixed dielectric constant ($\epsilon_{r\text{mix}}$) of 42. But in reality, moisture with $\epsilon_r = 80$ (approx.) would be absorbed into the body of the dielectric causing a dramatic increase in the value of $\epsilon_{r\text{mix}}$. This increase in $\epsilon_{r\text{mix}}$ will also increase the electrical energy, which increases the value of capacitance.

4.4.5 Varying Electrode Width (W_e)

As there is a flexibility to change the electrode width (W_e) in a wide range, it is wise to determine the number of fingers in the 1 mm² sensor structure by varying the dimension W_e and keeping the dielectric width to the minimum, i.e. 5 μm . Number of total fingers is equal to that of polyimide channels, where their lengths will be the same too. The importance behind this measure lies in the fact that the sensor signal is not only dependent on the characteristics of a single electrode pair, but also on the combination of all pairs.

Table 4.9: Results: Varying W_e on Model11 with W_p at a minimum.

W_e – electrode width (μm), C – capacitance (pF per length) for a single pair, n – # of fingers, L – length of a finger (μm), C_t – total capacitance (pF) in the whole sensor

Model	W_e	C	n	L	C_t
Model10	5	112	188	450	9.5
Model11	10	112	124	435	6
Model12	15	112	92	420	4.3

Figure 4.11 shows the relationship between electrode width and total capacitance of the sensor. In Table 4.9 the calculations for different W_e are shown. (Electrical energy is calculated assuming $\epsilon_{r\text{mix}} = 42$). The table reveals some important aspects:

- For a specific sensor area, increase in its electrode width decreases the number of pairs. Therefore, total capacitance of the whole sensor decreases as the number of pairs decreases. But for the single pair in 2D simulation, capacitance per unit length for different W_e was found to remain around a similar value.
- Thus a conclusion can be drawn that with a fixed W_p , variation in W_e influences the number of pairs of electrode/channel, not the capacitance per unit length. But variation in number of pairs, in fact, is influencing the final capacitance (C_t) of the sensor. Although the smallest electrode width is seen to result in the largest final capacitance, again a width smaller than 5 μm is not recommended for microfabrication [39].

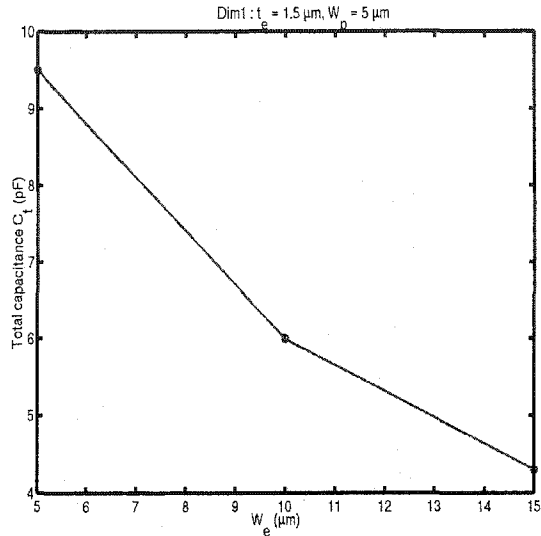


Figure 4.11: Total sensor capacitance against electrode width.

4.5 Grid Resolution and Time Step Resolution

In the whole parameter study for different 2 D models finite element simulations were tested with a number of triangular elements ranging from around 1200 (approx. 620 nodes) to 86000 (approx. 43000 nodes) for the types of Dim1. In case of different types of Dim4 this range was from around 15000 (approx. 7500 nodes) to 60000 (approx. 30000 nodes). There were no significant changes noticed in output results over this range of grid resolutions and, thus, grid convergence was ensured.

In addition, all simulation results were checked for time step convergence as well. Three different time steps (.01, .02, .005) generated the same output values to the third significant digit.

4.6 Analytical Verification

In order to verify the reliability of the numerical simulations performed in the study, a series of simplified 1 D versions of the main physical problems will be solved analytically. To satisfy the 1 D condition a model named Model1 is picked for the analytical calculation for both diffusion and electrostatic cases. Model1 (see Figure 4.12) is a Dim1 type of sensor with large dielectric width, electrode height, $t_e = 1.5 \mu\text{m}$ and polyimide height above electrode, $t_p = 0.25 \mu\text{m}$.

In addition, a similar analytical verification of the heat transfer results shown in Appendix B.

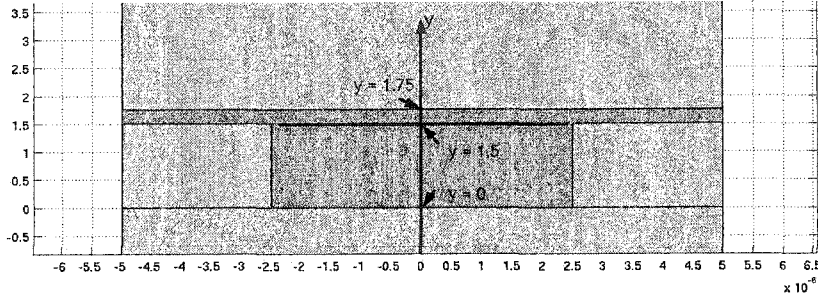


Figure 4.12: Model for analytical calculations.

4.6.1 Diffusion

For comparison with the analytical solution for the transient mass transfer process a particular case of Dim1 was simulated with the same grid and time step resolution as used in the parameter study. The selected geometry for the comparison has dielectric width $W_p = 5 \mu\text{m}$, electrode width $W_e = 5 \mu\text{m}$ and the same electrode height $t_e = 5 \mu\text{m}$ and additional polyimide height, t_p as mentioned above. The time time dependent concentration profile is obtained through FEMLAB at the median line of the effective subdomain (see Figure 4.12). The line is defined as the y axis, the origin $y = 0$ is set at the bottom surface of the effective subdomain and $y = L$ is the point at the top surface of the polyimide layer. The simulation results for the mass concentration profiles along y at different simulation time is shown in Figure 4.13. These profiles allow the extraction of mass concentration values at a particular point ($y = 1.5 \mu\text{m}$, top of effective subdomain) as a function of time. These results, expressed in % of relative humidity, are plotted as a dashed line in Figure 4.14.

For the analytical solution, if c_s is the mass concentration (%) at the surface, c_0 is the mass concentration (%) at time $t = 0$, and $c(t, y)$ is the mass concentration at point y at any time t , the initial and boundary conditions for this 1 D diffusion problem along y are as follows:

1 D diffusion equation:

$$\frac{\partial c}{\partial t} = \frac{\partial^2 c}{\partial y^2} \quad (4.1)$$

$$\text{at } t = 0, c = c_0 = 0$$

$$\text{at } y = 0, c = \frac{\partial c}{\partial y} = 0$$

$$\text{at } y = L, c = c_s = .95$$

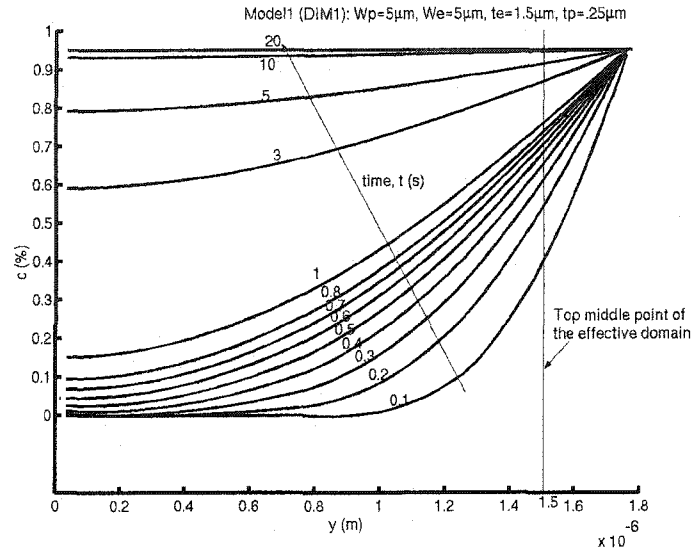


Figure 4.13: Simulation results in a cross section line plot along the vertical line at the middle of the model.

Solution

The solution [28] for this problem is as follows:

$$\frac{c - c_s}{c_0 - c_s} = \sum_{k=1}^n \frac{2(-1)^n}{(n + \frac{1}{2})\pi} \cdot e^{-(n+\frac{1}{2})\pi^2 F_0} \cdot \cos(n + \frac{1}{2})\pi \frac{y}{L} \quad (4.2)$$

Where $n = 50$ (found to be sufficient to ensure accuracy of 10^{-5}), $F_0 = Dt/L^2$, diffusion coefficient of polyimide, $D = 5 \cdot 10^{-13}$, time, t (s), length of the 1 D diffusion, $L = 1.75 \mu\text{m}$, y is any point (for the present calculation $y = 1.5 \mu\text{m}$, the point on y axis at the top surface of effective domain).

The analytical and simulation results for mass concentration over time at point $y = 1.5 \mu\text{m}$ are shown for comparison in Figure 4.14. The plot shows that at $t = 0$, mass concentration, $c = c_0$ and at $t \geq 10.7$ s, c reaches c_s . These results are able to approximately represent the results in simulation for the corresponding position (at $y = L$). The plot also shows that the analytical solution reaches the steady-state value faster than the numerical simulation, which is to be expected because of the incorporation of 2 D effects by the simulation.

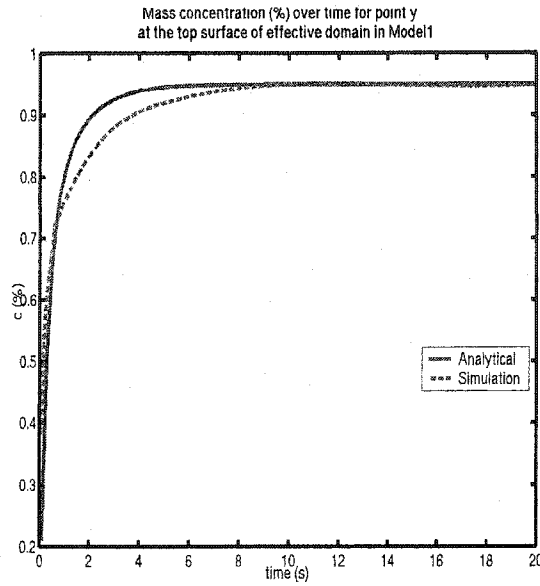


Figure 4.14: Time dependent analytical and simulation diffusion solution for the point on y at the top of the effective domain in Model1.

4.6.2 Electrostatic

For the verification of the capacitance calculation, a parallel plate capacitor is approximated. For Model1 (see Table 4.6), the simulation value of electrical energy (W) in the effective subdomain is $13.97 \cdot 10^{-10}$ J/m. By equation 2.15 we can find the value of capacitance, $C = 112$ pF/m, as shown in the table.

For the analytical solution if the dielectric area, A and distance, d can be calculated, equation 2.4 is sufficient to solve the capacitance in a 1 D approximation of Model1. By using eqn. 2.4. The analytical results for Model1 are as follows:

$$C = 1.116 \cdot 10^{-10} \text{ F/m} = 111.6 \text{ pF/m}$$

$$W = 1.395 \cdot 10^{-9} = 13.95 \cdot 10^{-10} \text{ J/m}$$

These analytical results agree well to those obtained from the simulation for Model1.

4.6.3 Thermal

The surface temperature (T_s) should be calculated in steady state condition to verify the value with simulation results. T_s can be calculated using following heat equation applied to the domain (see Figure 4.15) of the sensor system:

$$h(T_s - T_\infty) = q'' \quad (4.3)$$

Where h is the convection heat coefficient of the surrounding air at ambient temperature T_∞ and q'' is the heat flux provided by the microheater. In the simulation $h = 10 \text{ W/m}^2\text{K}$ and $T_\infty = 35^\circ\text{C}$ with a uniform heat flux, $q'' = 345 \text{ W/m}^2$ warmed up the polyimide surface to a steady state surface temperature, $T_s = 69.5^\circ\text{C}$ (see Figure B.1 in Appendix B, first case).

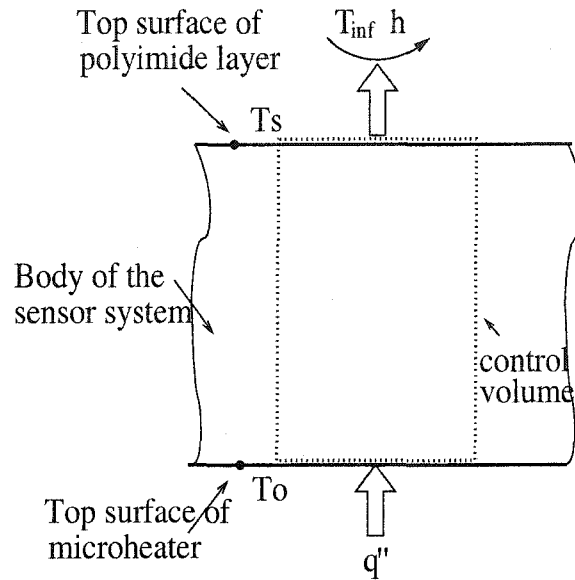


Figure 4.15: Thermal domain in the sensor system.

If a control volume is assumed as shown in Figure 4.15, by using the above heat equation with the prescribed values for a heat flux of 345 W/m^2 , the steady-state temperature results :

$$T_s = 69.5^\circ\text{C}$$

This value is the same value obtained for the steady-state surface temperature in the simulation for thermal resetting of the humidity microsensors.

4.7 Summary of Results

Summarizing the parameter studies presented in this chapter, the following parameter values optimize response time and output signal :

- Surface Geometry: a dome-shape surface represented by Dim4.
- Dielectric Width (W_p): the smaller the better in compliance with the dielectric strength, but $5 \mu\text{m}$ is a practical minimum for microfabrication.

- Electrode Height (t_e): the larger the better, but benefits start reducing at $1.5 \mu\text{m}$, while cost becomes a issue, so that $1.5 \mu\text{m}$ would be recommended.
- Electrode Width (W_e): the smaller the better for a constant sensor size, but $5 \mu\text{m}$ is a practical minimum for microfabrication.
- Height of Polyimide layer above Electrodes (t_p): as small as possible.

Chapter 5

Microfabrication

Following the conclusions of the parameter studies, preparations were made for the microfabrication of a series of sensors that would allow for the experimental validation of the preceding numerical analysis. Unfortunately, the original intent of bringing the manufacturing of prototype sensors based on the parameter study to completion could not be fulfilled. A series of setbacks caused by unreliable functioning of the pattern generator software to convert the microstructure layout and by a major upgrade work that stalled the nanofabrication facility for more than 2 month prevented the inclusion of an experimental validation in this study.

This chapter describes the preliminary steps accomplished in the manufacturing process, as well as recommendations of protocols for the microfabrication of the special dome-shaped surface revealed as best in the parameter studies.

5.1 Selection of Specimens

Based on the thorough study on parameters, dimensions of the test specimens for an experimental validation study are decided as follows:

1. $t_e = 1.5 \mu\text{m}$
2. $W_p = 5 \mu\text{m}, 10 \mu\text{m}$
3. $W_e = 5 \mu\text{m}, 10 \mu\text{m}, 15 \mu\text{m}$

Accordingly, the sets of specimens for micromachining are listed in Table 5.1.

5.2 Selection of models to be micromachined

Three types of MEMS structures for interdigitated electrodes can be considered for micromachining. Keeping the overall size of the structure the same, this approach allows

Table 5.1: Specimens for micromachining.

W_e – electrode width (μm), W_p – dielectric width (μm)
 t_e – electrode height = $1.5 \mu\text{m}$

Set	Specimen name	sensor size	W_p	W_e
Original x1	1 mm×1 mm	spec11	5	5
		spec12	5	10
		spec13	10	5
Original x2	2 mm×2 mm	spec21	10	10
		spec22	10	20
		spec23	20	10
Original x3	3 mm×3 mm	spec31	15	15

for the testing of some variations in the length of electrode fingers, along with testing an array of sensors instead of a single sensor. This approach can ensure whether there would be any practical influence of the length of electrode fingers or of the number of capacitors on the expected output signal. These structures can be seen in Figure 5.1 to Figure 5.3, accordingly:

1. A full MEMS structure with a single sensor/capacitor (Figure 5.1)
2. An array of 3 sensors/capacitors in a full MEMS structure (Figure 5.2)
3. An array of 4 sensors/capacitors in a full MEMS structure (Figure 5.3)

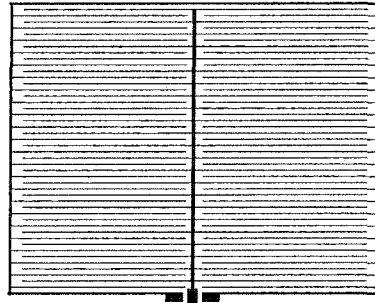


Figure 5.1: A full MEMS structure.

A combination of desired dimensions applied on these three structures leads to a cell (see Figure 5.4) of 6 sensors. A total number of eight cells would then be placed on a single wafer with 1 inch by 1 inch working area. This arrangement is made together with electric contact lines for input voltage. A designed layout of the sensor circuit can be seen in Figure 5.5.



Figure 5.2: Three sensors in a full MEMS structure.



Figure 5.3: Four sensors in a full MEMS structure.

5.3 Micromachining in MicroFab Lab

Micromachining of the specimens can be performed step by step following the sequence below:

1. Designing the layout of sensor design with layout editor L-Edit.
2. Making the mask in pattern generator.
3. Transferring pattern to a gold structure on to a silicon substrate.
4. Dispensing polyimide on the MEMS structure.
5. Giving the polyimide surface a desired shape .
6. Curing of polyimide.
7. Etching away polyimide from the top of connection points.

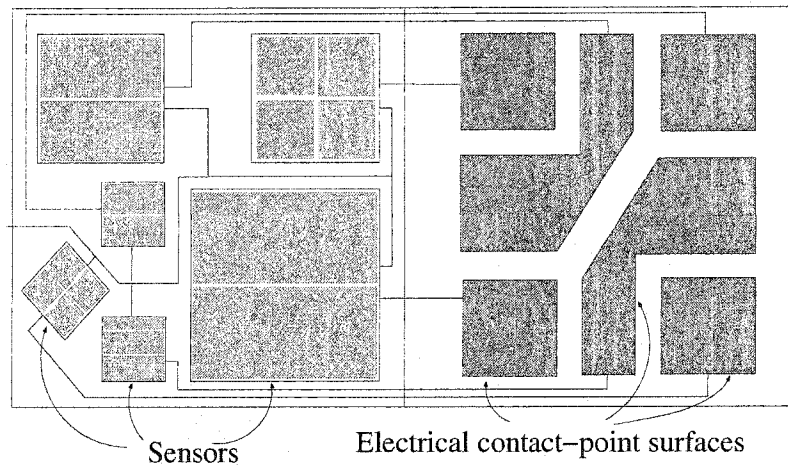


Figure 5.4: One cell composed of 6 sensors structure. Electrical connection points are seen on the right half of the cell.

First two steps were performed successfully, hence, the methods were noted but for other steps the recipes can be recommended. The protocols for different steps are described in the following subsections:

5.3.1 Ledit

An 1 inch \times 1 inch layout of the microstructure is generated by L-edit. In total 48 different sizes of sensor structures were included with different features. In total 8 cells occupied the whole area, where each cell was made up of 6 sensor structures with 8 electrical contact surfaces. Minimum feature size was only 5 μm . A total of 48 electrical contact surfaces were included so that all sensors would have their own contact surface to voltage applied. A common ground contact surface was included for all the sensor microstructures.

The layout was at first written to a file with extension .tdb and then exported to GDS II file with extension .gds. This GDS II file could be recognized by the mask generator employed in the microfabrication facility.

5.3.2 Mask making

It was chrome mask blank where the pattern generator (mask generator) wrote the whole layout imported from L-edit.

Pattern generator

The pattern generator employed was the Heidelberg Instruments DWL66. It is a high resolution pattern generating system for fabricating photomasks. The step by step method [26]

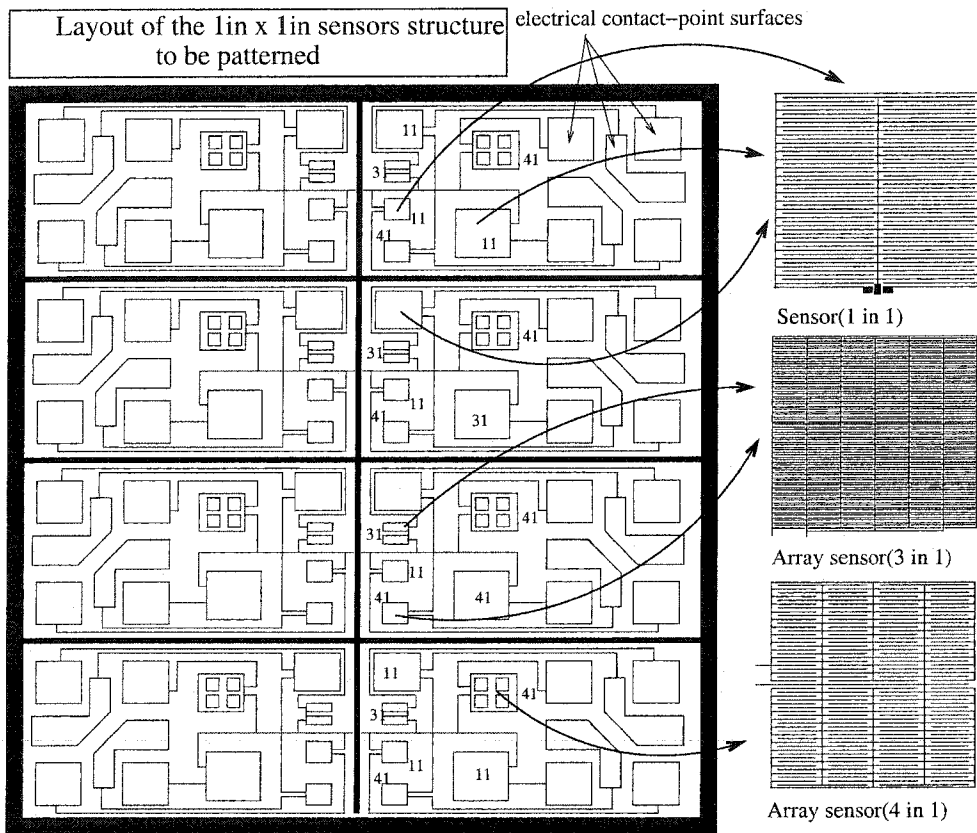


Figure 5.5: 8-cells layout of the combined structure on a wafer.

used to generate the pattern is given below:

1. At first GDS II file was imported from the layout editor. Once GDS II file was imported it was converted to the 'LIC' file format. DWL66 is only capable of reading the 'LIC' file format.
2. After transferring the converted file to the DWL66 system, appropriate configuration on the instruments was done in accordance with the writing manual of DWL66.
3. A complete set-up of the pattern generator was performed by its interfacing software. The generator commenced the writing after it was asked to expose from the 'job menu' in the DWL66 software.
4. After the job was done the mask was unloaded from the generator and brought to the developing and etching tables.

The specifications used for generating the pattern were:

- 4 Beam / 4 mm
- Laser power: 104.912 mW
- Tube current: 45.6 A
- Tube voltage: 230 volts
- Total time taken: 11 min 57 s

Mask developing

- Developer: 354 developer
- Time: less than 50 s as minimum feature size = 5 μm
- Temperature: 18°C
- Inspection under microscope

Chrome etching

- Etchant: NanoFab Chrome Etchant
- Etch time: less than 50 s as minimum feature size = 5 μm
- Temperature: 18°C
- Inspect under microscope

If minimum feature size is less than $5\ \mu\text{m}$ both developing and etching duration should be decreased to 20-25 s. Then the mask should be inspected under microscope, developed or etched more if needed. All steps up to this point were successfully completed at the Nanofabrication Facility, University of Alberta. The following subsections describe a series of recommendations for transferring the pattern, dispensing polyimide and generating the desired surface shape of polyimide. All of these recommendations were collected from literature and from discussions with experts.

5.3.3 Pattern transfer: microheater and microsensor structures

In order to prevent any amount of heat conducted through the substrate, a thermal insulator is necessary. An electrical insulator is essential in this system to avoid electrical short circuit. The polysilicon microstructure of the heater should be immersed in this insulator material. The protocols to deposit these layers at the time of transferring patterns are as follows [18, 20]:

- A $0.2\ \mu\text{m}$ thick thermal insulator (Si_3N_4) layer is deposited on a silicon substrate by LPCVD method.
- For the microheater an LPCVD polysilicon layer with a thickness of $0.6\ \mu\text{m}$ is deposited on the top of Si_3N_4 layer and then doped.
- With a mask of the heater microstructure (made by the same recipe above but with the heater microstructure layout), the polysilicon layer is patterned to form the integrated heater.
- The contact points (surfaces), which are extended out of the heater area, are opened using reactive ion etching.
- A layer of electrical insulator (LTO) is then deposited on the wafer. This deposited layer should be of $1.1\ \mu\text{m}$ thickness so that actual layer of LTO on the top of the heater would be of $0.5\ \mu\text{m}$.
- A layer of Gold (Au) of $1.5\ \mu\text{m}$ thick is then sputtered on the top of the LTO layer.
- The pattern of the interdigitated electrodes for the capacitive sensor is transferred to the Gold layer by using the mask prepared.
- The electrical contact surfaces are then opened by using reactive ion etching.
- To investigate the need for electrical insulation a layer of LTO is not deposited immediately on the top of the Gold microstructure. At first it should be determined that without using this layer the sensor works. It means that the moisture saturated polyimide is assumed to be an electrically non-conducting material. If it is not, at this point a layer of LTO should be deposited with a minimum thickness close to $0.1\ \mu\text{m}$ according to the needs.

5.3.4 Dispensing polyimide and curing

After the Gold microstructure is prepared in a wafer, polyimide can be dispensed by following the method [5] below:

- Dispense the adhesion promoter (VM651) on the Gold microstructure when the wafer is static. The time duration is 3 s.
- Hold for 20 s.
- Spin dry for 30 s.
- Bake this adhesion promoter on a hotplate at 120°C for 30 s.
- Dispense the polyimide (PI2556) on the wafer when it is static. Hence polyimide is dispensed in the top of the baked adhesion promoter.
- Rotate the wafer at 500 rpm for 5 s.
- Rotate it at 2000 rpm for 30 s to get a polyimide layer thickness of 1.5 μm .
- Perform spin dry for 15 s.
- Soft bake the polyimide at 120°C for 30 s followed by 150°C for 30 s.
- Cure the polyimide in an oven using the following cure profile:
 - Put the wafer in an oven.
 - Heat from room temperature to 200°C, ramp rate 4°C/min in air.
 - Hold at 200°C for 30 min in air.
 - Heat from 200°C to 300°C, ramp rate 2.5°C/min in nitrogen.
 - Hold at 300°C for 60 min in nitrogen.
 - Cool the wafer gradually down to room temperature.

In the microfabrication process selection of Gold (Au) as the material of the MEMS structure and Si as the substrate was made for the ease of processability and reliability in micromachining. Gold, as a conductive material, has a well-established preference in semiconductor industries and, in addition, has good thermal and mechanical stability together with Si substrate at an elevated temperature. A good reason of using Gold is its robustness with moisture.

5.3.5 Providing a desired shape to the polyimide flat surface

If the polyimide is dispensed on the top of the microstructure and then cured at a prescribed temperature, a flat surface of polyimide can be obtained. For an initial experiment it may be useful, but to manufacture the desired sensor a dome-shaped polyimide surface has to be micromachined. This micromachining should be performed following the curing part. However, it happens to be a challenge to change the flat surface of polyimide into a dome-shape or even some similar shape. Two recipes are chosen as the most promising and detailed in the following sections.

- Melting a square tooth shape polyimide surface.
- Using an array of microneedles.

Step by step protocols for each of above two methods are given in the following subsections:

Melting a square tooth shape polyimide surface

1. Make a mask that would define a square tooth shape to the surface of the polyimide.
2. Apply appropriate photoresist on the top of the flat polyimide surface.
3. Transfer the pattern onto the polyimide by developing and etching photoresist and polyimide to obtain square tooth shape polyimide surface.
4. Elevate the temperature near the melting point of polyimide.
5. Wait until the rectangular-shaped peaks turn into some expected dome-shaped peaks.
6. Cool down the polyimide to solidify the shape.
7. Cure the polyimide at the prescribed temperature.

Using an array of microneedles

Peter Lucke in his work [21] developed micro-needles for intracellular applications. His work in fact inspired the use of an array of very tiny microneedles to provide a required dome-shape surface to the sensor. A simplified method useful for the present work could be extracted from his paper as follows:

1. Use a wafer with required thickness.
2. Apply an appropriate photoresist (AZ4640) to define the needles and release trench.
3. Make a mask that would define the needles with protection pillars around each of the needle.

4. Transfer the pattern to the wafer after developing and needle pillars are obtained by Deep Reactive Ion Enhanced (DRIE) Etching.
5. To sharpen the needle pillars and to release the completed device the wafer is placed in an Reactive Ion Enhanced (RIE) etcher with an SF₆ plasma. This RIE etching is performed maintaining certain angle to the pillars.
6. During the sharpening, the protection pillars that surround the needles are totally etched away.
7. Etch away the remaining silicon at the bottom of the trench for the release.
8. The mask should be prepared in such way that an array contains as many needles as possible.
9. Now the sensor should be heated up near the melting point of polyimide already dispensed on it.
10. This array of silicon needles is then held upside down so that the tips of needles point downwards vertically.
11. Now press the needles against the soft polyimide and then lift off several times so that the whole surface is full of cone-shaped pits equally apart from each other.
12. Cool down the polyimide and obtain cured polyimide with a dome-shaped surface.

For alternative methods proposed for micromachining the desired polyimide surface, such as dispensing polyimide in a sonic bath and deposition of polyimide by GLAD, see Table A.1 in Appendix A.

Chapter 6

Conclusion

The present project consisted of the numerical development of a humidity microsensor, which has a short response time with high sensitivity. This humidity microsensor is being developed at the Aerosol Research Laboratory of Alberta (ARLA) and is expected to be useful in human lungs to measure humidity inside the airways. The response time is found to be less than .4 s with the selected type of design. This will allow it to complete a measurement cycle of less than 1 s in order to start the next cycle. The project development involved literature review, microstructure and material selections, design, simulations, parameter study, results analysis and manufacturing preparations. The summary can be presented in the following paragraphs.

A thorough literature review on microsensors and materials led to the choice of the film polymer capacitive method for the sensor and of cross-linked polyimide as the dielectric. An interdigitated electrode structure was chosen for the design. This structure was found to be best suited for the present development. After a long search for the best polyimide for our research, HD Microsystems provided a suitable type, considering all properties of polyimide relevant to our project, which is called PI2556. PI2556 has been used as a dielectric in semiconductor industries for a long time and shown to have considerable amount of moisture uptake.

A parameter study was necessary to reveal the influences of dimensions and parameters on the physics of processes involved. The result of the analysis produced the correct and optimized dimensions of the sensor to satisfy the objective of the present development. A dome-shaped air-contact surface of polyimide was found to provide the shortest response time. The response time was simulated to be less than .4 s. Several dimensions of the design could be optimized after a thorough analysis to achieve better and sufficiently strong output signal for practical measurements. In total ten types of models were involved in the simulation and one of them (Dim4) turned out to be preferred. In model Dim4 the rate of water vapor accumulation in the polyimide dielectric was found to be almost two times faster than with other models. This is due to its vast contact area open to air. Dim4 has a special dome-type surface that expedites water vapor diffusion into the dielectric layer in a very short span of time. On the other hand dome-type surfaces ben-

efit from having an effective subdomain with least amount of no-polyimide area, which is expected to result in stronger electrical signal. Therefore, this model showed the highest sensitivity. An input voltage of less than the dielectric strength (breakdown voltage) resulted in reasonable estimates of signal in the order of pF, which comply with practical capacitance values in submillimeter level systems.

Absorption is always faster than desorption when moisture and an absorbent are in the diffusion process. For this reason it is necessary to force the diffused water out at the end of a measurement cycle in the presently developed humidity sensor. The desorption process will be accelerated by an external force (heat) and this will reset the sensor for the following measurement cycle. A simulated microheater showed that a reasonable range of heat is sufficient to successfully heat up the sensor body in less than .1 s.

After attaining a certain decision from results of the simulations, several methods were studied for the purpose of providing the polyimide film a dome-shape surface by micromachining. Melting square shape ripples into dome-shaped, and using a microneedles array, dispensing polyimide in a sonic bath, deposition of polyimide by GLAD among others are revealed to be some potential micromachining methods. Thus, a complete preparation was done towards the goal to micromachining the sensor in a microfabrication facility. This preparation will be helpful for future researchers to move faster towards the start of manufacturing. As a follow-up to the development, manufacturing has to be done in a modern fabrication facility and *in vivo* tests should be conducted on laboratory animals and subsequently inside the human lung.

In a development strategy, for the sensing of a physical parameter of interest, it is necessary to use various structures of the design and also to analyze the design under different sensing principles. Partially, the study could cover the purpose of walking through various structures towards the application of different sensing principles. This study compared various shapes and dimensions of a capacitive humidity microsensors to minimize response time and maximize sensitivity.

Appendix A

Tables

Table A.1: Additional methods of micromachining surface of polyimide film.

#	Methods	Procedures
1	Polyimide flat surface	Dispensing polyimide on the substrate by spinning it over at a certain speed. The film is cured at a prescribed temperature. This way a flat surface polyimide can be obtained. If no other type of surface can be obtained, this would serve as a standard specimen for experiments.
2	Glancing angle deposition (Glad) [41]	a) It is an electron beam evaporation technique with oblique vapor incidence on the substrate placed vertically tilted by a certain angle, b) it exhibits structural anisotropy, c) usually deposited materials are: SiO ₂ / Ti films / Glass, d) the film density is controlled by rotating the substrate during this oblique deposition of thin film. Controlling density helps to reduce the effects of anisotropic shadowing, leading to columns that exhibit a more symmetrical cross-sectional shape, e) although Wu et al., in their works [40, 41], demonstrated that SiO can be deposited as a dielectric by the application of Glad, it is still a concern to deposit polymer by this method, f) moreover, an anisotropic structure can induce corresponding anisotropy in the optical, magnetic, and electrical properties of films. As a result, anisotropic correlations may be needed, which will make the design more difficult.
3	Sonic Bath Spinning	Dispensing of polyimide can be performed in a sonic bath which has a control of a range of frequency. Controlling the operating frequency would control the amplitude of the ripples on top of polyimide surface. Still it is difficult to say whether this method would work, because it may be difficult to provide both floating and spinning at the same time. But it would give a promising result if it could be applied in a high frequency.

Table A.2: Material properties [24, 5] used in the simulation.

E – Young’s modulus, ν – Poisson’s ratio, ρ – Density, C – Heat Capacity, k – Thermal conductivity, D – Diffusion coefficient, σ – Electrical conductivity, ϵ_r – Dielectric constant

name	E GPa	ν	ρ kg/m ³	C J/kg·K	k W/m·K	D m ² /s	σ ohm ⁻¹ m ⁻¹	ϵ_r
Polyimide	2.45	.41	1400	1200	.25	5e-13	3.3e-14	3.5
Substrate	68	.19	2180	750	1.38	0	2e-14	4.5
Gold	80	.42	19320	900	301	0	4.5e7	5

Table A.3: List of polyimides with specifications.

Company names – AC (BP Amoco Chemicals), HDM (HD Microsystems)

E – Young’s modulus, T_g – Glass transition temperature, t – Thickness, CTE – Coefficient of thermal expansion (ppm/°C), ϵ_r – Dielectric constant, m – Moisture uptake

Product	Company	t (μ m)	Cure (°C)	T_g (°C)	CTE	E (GPa)	ϵ_r	m (%)
Ultradel	AC	2+	300		24	3.5	3.5	3.4
PI2556	HDM	.7 – 1.5	295	325	50	2.5	3.3	3
PI2575	HDM	2 – 4	295	320	50	2.5	3.3	
PI2723	HDM	2 – 4	350	310	57	2.5	2.9	<1.1
PI2737	HDM	1.5 – 4	375	350	16	4.7	2.9	<1.1
PIX1400	HDM	1 – 2.5	350	290	50	3		1.1
PI2545	HDM	1 – 3	375	400	13	2.3		
PIXL110SX	HDM	1.5 – 3	350	360	10	4.6	2.9	.5
PI2610	HDM	1 – 3	350	360	3	8.5	2.9	.5
PI2616	HDM	.7 – 2	350	360	3	8.5	2.9	.5
PIX6400	HDM	1 – 5	350	270	50	3		

Appendix B

Figures

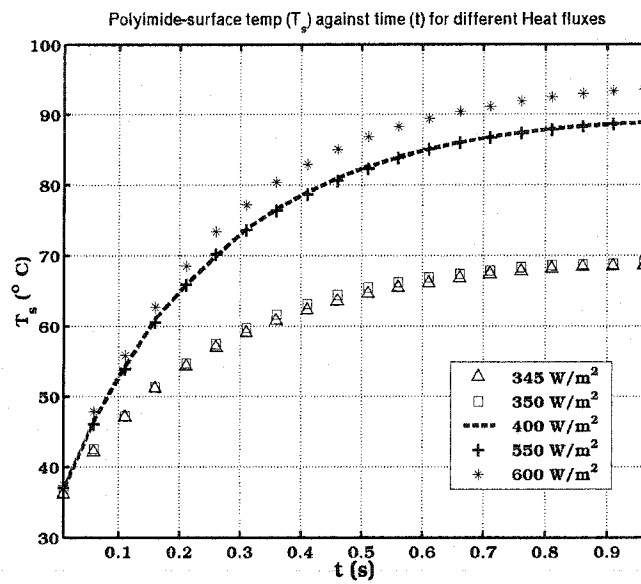


Figure B.1: Air contact surface temperature with time for different heat fluxes generated by the microheater.

Appendix C

Matlab Codes

The Matlab codes below are part of a file (Model41_05jun03.m) imported to the Matlab workspace from FEMLAB. This part was modified to extract the integrated values in all time steps at a time. This printout shows the modified parts and other parts relevant for the context.

```
% FEMLAB Model M-file
% Generated 05-Jun-2003 18:28:19 by FEMLAB 2.2.0.181.

flclear fem
% FEMLAB Version
clear vrsn;
vrsn.name='FEMLAB 2.2';
vrsn.major=0;
vrsn.build=181;
fem.version=vrsn;

% Recorded command sequence

% New geometry 1
fem.sdim={'x','y'};

...
...
% Solve dynamic problem
fem.sol=femtime(fem,...
'tlist', 0:0.01:2,... %fem.sol.tlist contains the time steps
'atol', 0.001,...
'rtol', 0.01,...
'jacobian','equ',...
'mass', 'full',...
'ode', 'ode15s',...
'odeopt', struct('InitialStep',{[]},'MaxOrder',{2},'MaxStep',{[]}),...
'out', 'sol',...
'stop', 'on',...
'init', 'init',...
'report', 'on',...
'timeind','auto',...
'context','local',...
'sd', 'off',...
'nullfun','fnullorth',...
'blocksize',5000,...
'solcomp',{'V','C'},...
'linsolver','matlab');

% Save current fem structure for restart purposes
```

```

fem0=fem;
% Plot solution
postplot(fem,...
'geomnum',1,...
'context','local',...
'tridata',{'c','cont','internal'},...
'trifacestyle','interp',...
'triedgestyle','none',...
'trimap','jet',...
'trimaxmin','off',...
'tribar','on',...
'geom','on',...
'geomcol','bginv',...
'refine',3,...
'contorder',2,...
'phase',0,...
'title','Time=2 Surface: concentration (c) ',...
'renderer','zbuffer',...
...
...
...

% Integrate on subdomains
%% MODIFIED coding to extract integrated mass concentration for all time steps
for i=1:length(fem.sol.tlist) % tlist-list of time steps stored in vector fem.sol
Irh(i)=postint(fem,'c',... %Irh-vector is assigned to carry the integrated mass
'cont','internal',... %concentration in subdomain 3
'contorder',2,...
'edim',2,...
'solnum',i,...
'phase',0,...
'geomnum',1,...
'dl',3,... % effective subdomain (3) to be integrated
'intorder',4,...
'context','local');

% MODIFIED coding to extract integrated electric energy for all time steps
Iwe(i)=postint(fem,'We',... % Iwe-vector containing the integrated We in subdomain 3
'cont','internal',...
'contorder',2,...
'edim',2,...
'solnum',i,...
'phase',0,...
'geomnum',1,...
'dl',3,... % effective subdomain (3) to be integrated
'intorder',4,...
'context','local');
end

```

MATLAB coding to process data, calculate response time and plot desired output diagrams for Diffusion

```

%% Matlab coding to call fspline function and plot water vapor mass
%% against time till response time [for both total and effective subdomains]

load data01.dat; %data01 contains a list of integrated mass concentration
%corresponding to each time step

m=length(data01(1,:));
t=data01(:,1);
set=m-1;
p=0;
for k=1:2
j=0;
for i=k+1:2:set
p=p+1;

```

```

j=j+1;
c=data01(:,i);
[tr,cr]=fspline(t,c); % calling the function 'fspline'
ncr=length(tr);
figure(k);

dimtab(p,1)=j;
dimtab(p,2)=tr(ncr); % tr contains time steps up to the response time
dimtab(p,3)=cr(ncr); % cr contains integrated mass concentration values
                    % corresponding to vector tr

plot(tr,cr);
hold on;

end
end
%..... FUNCTION fspline .....
% function fspline to find out response time and present it by cubic spline interpolation
function [tr,cr] =fspline(t,c)
c=49e9*c; % coverting mass concentration (m^3) into vapor mass (micro-gram)
tt = 0:.0001:2;
    cc = spline(t,c,tt);
    length(cc);
    length(tt);
    n=length(tt);
    for r=1:n
        if roundn(cc(r),-3)==roundn(.90*cc(n),-3)
            indx=r;
            tr=tt(1:indx);
            cr=cc(1:indx);
            break
        end
    end
end

```

MATLAB coding for Analytical calculations for Diffusion

```

%%% coding for analytical diffusion calculations %%%

cs=.95; % surface concentration (%)
c0=0; % initial condition
L=1.75e-6; % length of the 1 D domain of Modell
D=5e-13; % diffusion coefficient
y=1.5e-6; % position of interest, presently at the top surface
% of the effective domain
r=y/L; % dimensionless ratio
m=51; % m = n-1
k=0;
for t=.1:.2:20 % for loop to store data for different time steps
f0=D*t/L^2; % fourier no
sr=0;
k=k+1;
tm(k)=t; % tm is the vector representing time steps
for i=1:m
n=i-1;
sri=((2*(-1)^n)*(exp(-(n+.5)*f0*pi^2))*cos(n*pi*r+.5*pi*r))/(n*pi+.5*pi);
sr=sr+sri;
end
c=cs+(c0-cs)*sr; % calculating the solution for c of position y at t
vec(k)=c % solution vector for c
end
plot(tm,vec) % plot concentration (%) against time
xlabel('time (s)'), ylabel('c (%)');
title('Mass concentration (%) over time for point
y at the top surface of effective domain in Modell ')

%~~~~~ END ~~~~~

```

Bibliography

- [1] A. Ahsan, C. F. Lange, and W. Moussa. A multisensor microprobe to map conditions in the human airways. In *3rd Alberta Biomedical Engineering Conference*, number 20, Canada, 2002. BME, University of Alberta.
- [2] A. Ahsan, C. F. Lange, and W. Moussa. Development of a humidity microsensor with thermal reset. In Walied Moussa, editor, *MEMS, NANO, and Smart Systems*, pages 89–93, CA USA, 2003. IEEE CAS, IEEE Computer Society.
- [3] L.K. Baxter. *Capacitive Microsensors, Design and Applications*. IEEE Press, New York, 1997.
- [4] A. S. Castela and A. M. Simoes. Assessment of water uptake in coil coatings by capacitance measurements. *Journal of Corrosion Measurement (JCM)*, 1(2), 2001.
- [5] John Craig. *Product Information, Pyralin PI2555 Series*. HD MicroSystems, CA USA, 2003.
- [6] J. Crank and G. S. Park, editors. *Diffusion in Polymers*. Academic Press Inc., London, 1968.
- [7] E. Daviskas, I. Gonda, and S. D. Anderson. Mathematical modeling of heat and water transport in human respiratory tract. *J. Appl. Physio.*, 69:362–372, 1990.
- [8] K. Domansky, J. Liu, L. Wang, M. H. Engelhard, and S. Baskaran. Chemical sensors based on dielectric response of functionalized mesoporous silica films. *Journal of materials research*, 16(10):2810–2816, 2001.
- [9] A. D. Eisner and T. B. Martonen. Design and development of a micro-thermocouple sensor for determining temperature and relative humidity patterns within an airstream. *Transactions of the ASME. Journal of Biomechanical Engineering*, 111:283–297, 1989.
- [10] G. A. Ferron, B. Haider, and W. G. Kreyling. Inhalation of salt aerosol particles – I. Estimation of the temperature and relative humidity of the air in the human upper airways. *J. Aerosol Sci.*, 19:343–363, 1988.
- [11] W. H. Finlay. *The Mechanics of Inhaled Pharmaceutical Aerosols: An Introduction*. Academic Press, London, 2001.

- [12] J. W. Gardner. *Microsensors: Principles and Applications*. Wiley, New York, 1994.
- [13] J. W. Gardner, V. K. Varadan, and O. O. Awadelkarim. *Microsensor MEMS and Smart Devices*. John Wiley & Sons, Ltd, England, 2002.
- [14] D. J. Griffiths. *Introduction to Electrodynamics*. Prentice Hall, USA, 3rd edition, 1999.
- [15] L. Hartshorn, N. J. L. Megson, and E. Rushton. The structure and electrical properties of protective films. *Journal of the Society of Chemical Industry, Chemistry & industry*, 56:266r, 1937.
- [16] HD MicroSystems, CA USA. *Polyimides for Microelectronics, Product Selector Guide*, 2003.
- [17] F. P. Incropera and D. P. DeWitt. *Introduction to Heat Transfer*. John Wiley & Sons, USA, 3rd edition, 1996.
- [18] U. Kang and K. D. Wise. A high-speed capacitive humidity sensor with on-chip thermal reset. *IEEE Transaction on Electron Devices*, 47:702–710, 2000.
- [19] L. D. Landau and E. M. Lifshitz. *Electrodynamics of Continuous Media*, volume 8 of pp. 7189–7194. Pergamon Press Ltd., London, 1st edition, 1960.
- [20] C. Laville, J. Y. Delétage, and C. Pellet. Humidity sensors for a pulmonary function diagnostic microsystem. *Sens. Actuators B*, 76:304–309, 2001.
- [21] P. Lucke. Silicon micro-needles with flexible interconnects and tip metallization for intracellular application. Master's thesis, University of Washington, USA, 2002.
- [22] M. Matsuguchi, E. Hirota, T. Kuroiwa, S. Obara, T. Ogura, and Y. Sakai. Drift phenomenon of capacitive-type relative humidity sensors in a hot and humid atmosphere. *Journal of The Electrochemical Society*, 7:2796–2799, 2000.
- [23] M. Matsuguchi, Y. Sakai, and N. Maeda. Competitive sorption of water vapor and CO₂ in photocrosslinked PVCA film for a capacitive-type humidity sensor. *Journal of Applied Polymer Science*, 83:401–407, 2002.
- [24] MatWeb. Material properties data. <http://www.matweb.com/>, May 16, 2002.
- [25] E. R. McFadden, Jr., B. M. Pichurko, H. F. Bowman, E. Ingenito, S. Burns, N. Dowling, and J. Solway. Thermal mapping of the airways in humans. *J. Appl. Physiol.*, 58(2):564–570, 1985.
- [26] NanoFab, University of Alberta, Edmonton AB Canada. *Instruction Manual for the Heidelberg Instruments DWL66 Laser Pattern Generator*, 2002.

- [27] H. Nieminen, V. Ermolov, K. Nybergh, S. Silanto, and T. Ryhanen. Microelectromechanical capacitors for RF applications. *Journal of Micromechanics and Microengineering*, 12:177–186, 2002.
- [28] M. Necati Ozisik. *Heat Transfer. A Basic Approach*. McGraw-Hill Book Company, New York, 1 edition, 1985.
- [29] R. Papazyan and R. Neimanis. Detection and localisation of water ingress in mass impregnated cables. *Nordic Insulation Symposium*, pages pp. 29–36, 2003.
- [30] W. Qu and J. Meyer. A novel thick-film ceramic humidity sensor. *Sensors and Actuators*, B:175–182, 1997.
- [31] W. Qu and J. Meyer. Thick-film humidity sensor based on porous MnWO_4 material. *Measurement science & technology*, 8:593–600, 1997.
- [32] Z. M. Rittersma and W. Benecke. A humidity sensor featuring a porous silicon capacitor with an integrated refresh resistor. *Sensors and Materials*, 12:35–55, 2000.
- [33] D. K. Roveti. Choosing a humidity sensor. *Sensors Online Magazine*, <http://www.sensorsmag.com/>, June 30, 2002.
- [34] School of Electrical and Computer Engineering, Georgia Tech. Diffusion. <http://www.ece.gatech.edu/research/labs/vc/theory/diffusion.html>, August 12, 2002.
- [35] J. Shake. *Active Device Technologies: The RF and Microwave Handbook*. CRC Press LLC, Boca Raton, electronic edition, 2001.
- [36] V. Vasilyev. Determination of the effective dielectric constant from the accurate solution of the poisson equation. *Journal of computational chemistry*, 23:1254–1265, 2002.
- [37] W. Volksen. *Encyclopedia of Materials: Science and Technology*. Number pp. 7189–7194. Elsevier Science Ltd., USA, e-book edition, 2001.
- [38] John G. Webster, editor. *Measurement, Instrumentation and Sensors Handbook*. CRC Press LLC, London, cd-rom edition, 1999.
- [39] K. Westra. Personal communication. Nanofabrication Facility, University of Alberta, May, 2003.
- [40] A. T. Wu and M. J. Brett. Sensing humidity using nanostructured SiO posts: Mechanism and optimization. *Sensors and Materials*, 13:399–431, 2001.
- [41] A. T. Wu, M. Seto, and M. J. Brett. Capacitive SiO humidity sensors with novel microstructures. *Sensors and Materials*, 11:493–505, 1999.